Crack onset and growth at the fibre-matrix interface under a remote biaxial transverse load. Application of a coupled stress and energy criterion

V. Mantič, I.G. García

Group of Elasticity and Strength of Materials, School of Engineering, University of Seville
Camino de los Descubrimienos s/n, 41092 Seville, Spain

Abstract

A theoretical model for prediction of the critical load generating a crack onset at the fibre-matrix interface under a remote biaxial transverse load is presented. In particular, this work is focused on the tension dominated failure. After an abrupt onset the crack grows unstably up to achieving an arrest length. A simple plane strain model of a single circular inclusion surrounded by an unbounded matrix allows to obtain conclusions approximately valid for a dilute fibre packing. Linear isotropic elastic behaviour is assumed for both inclusion and matrix. Two classical elastic solutions for both perfectly bonded and partially debonded circular inclusions are used together with a coupled stress and energy criterion, proposed recently in the framework of Finite Fracture Mechanics, and a phenomenological law for fracture toughness of interface cracks growing in fracture mixed mode. The obtained analytical and semi-analytical expressions make easy to study the influence of all the dimensionless parameters governing the fibre-matrix system behaviour: Dundurs elastic bimaterial constants α and β, the interface brittleness number γ, the load biaxiality parameter η, and the fracture mode-sensitivity parameter λ. A size effect of the inclusion radius on the critical load is predicted, smaller inclusions being stronger and less dependent on the secondary load. Finally, an experimental procedure for measurement of the fibre-matrix interface fracture and strength properties is proposed.

Keywords: composites, circular inhomogeneity, crack initiation, interface debond, size effect, finite fracture mechanics, fracture thoughness, damage mechanism, failure criteria, brittleness number

1. Introduction

Composites reinforced by long fibres are commonly used as a structural material in lightweight structures at present. In aerospace applications, where lightweight is a key aspect of the design, their level of structural responsibility has significantly increased as they are massively used in primary structures. However, our understanding of the damage mechanisms occurring in these composites on different scales is still insufficient. Thus, it is necessary to generate more knowledge about these mechanisms in order to avoid the present high level of uncertainty in the failure loads predicted in the design.

One of the most complex failure mechanisms on micro scale in these composites is associated to the matrix failure, also called inter-fibre failure. In particular, the tension dominated mechanism follows a well described sequence of stages, see Hull and Clyne (1996) and París et al. (2007): *i)* failure is initiated at the fibre-matrix interface as small debonds, *ii)* the interface cracks grow along the interface until a certain arrest angle and then *iii)* kink out the interface towards the matrix, *iv)* coalescence of growing matrix cracks generates a macrocrack which may cause the failure of the unidirectional lamina.

The present work is focused on the two first steps of this failure mechanism: crack initiation and growth at the fibre-matrix interface. Problem of a single fibre embedded in a matrix including a partial debond has been intensively studied by many authors for a long time, see París et al. (2007) and Mantič

Email addresses: mantic@esi.us.es (V. Mantič), israelgarcia@us.es (I.G. García)

(2009) for comprehensive reviews. Nevertheless, the debond onset has not attracted sufficient attention up to the last decade. Results presented in bibliography have usually been obtained by computational methods as cohesive zone or weak interface models, see for instance Carpinteri et al. (2005), Xie and Levy (2007), and Távara et al. (2011)). Mantič (2009) proposed a theoretical model to predict the crack initiation along the fibre-matrix interface under an uniaxial remote tension. This theoretical model is based on the coupled criterion introduced by Leguillon (2002) in the framework of the Finite Fracture Mechanics, see also Cornetti et al. (2006) and for a review Taylor (2007). This model proposes to apply both the stress and energy criteria simultaneously as a sufficient condition for the interface crack onset.

In the present work, an extension of the theoretical procedure developed by Mantič (2009) to the case of tension dominated remote biaxial transverse loads is developed. Note that the effect of the secondary compression in addition to a dominating tension has been demonstrated to be important by París et al. (2003) and Correa (2008). This analysis is carried out for dilute fibre packing where the influence of adjacent inclusions is almost negligible, whereas for dense fibre paking, a numerical method should be employed based on other solutions, e.g. Kushch et al. (2010). In addition, several models developed under the assumption of dilute fibre packing have demonstrated being useful to explain experimental results even for densely packed composites, see Correa (2008). After a revision of the solution of the elastic inclusion perfectly bonded to the matrix in Section 2, the elastic problem of an inclusion with a debond is analysed in Section 3, where a general analytical solution is simplified for this problem. Coupled criterion is developed and applied in Section 4 and the results for the critical crack length and remote load at the onset are obtained. Section 5 describes the influence of the remote secondary load and the inclusion size on the results obtained. Finally a new experimental procedure for an indirect measurement of the strength and fracture interface properties is presented in Section 6.

2. Stresses in a single inclusion under a remote biaxial transverse load

Stress based failure criteria usually consider the stress state prior to the damage appearance. Hence the aim of this section is to study the tractions along the fibre-matrix interface under remote biaxial load transverse to the fibre axis. Assuming certain hypothesis, a classical elastic solution is particularized for this problem providing closed form expressions of tractions. Finally, the traction dependence on the key problem parameters is discussed.

Consider a circular cylindrical inclusion of radius a embedded in an infinite matrix and perfectly bonded along its lateral interface. Let (x, y, z) and (r, θ, z) be suitably defined cartesian and cylindrical coordinate systems, the z-axis being coincident with the inclusion (longitudinal) axis. Remote uniform biaxial transverse load $(\sigma_x^\infty, \sigma_y^\infty)$ is applied parallel to the the two axes, x and y, transverse to the cylindrical inclusion axis, see Figure 1.

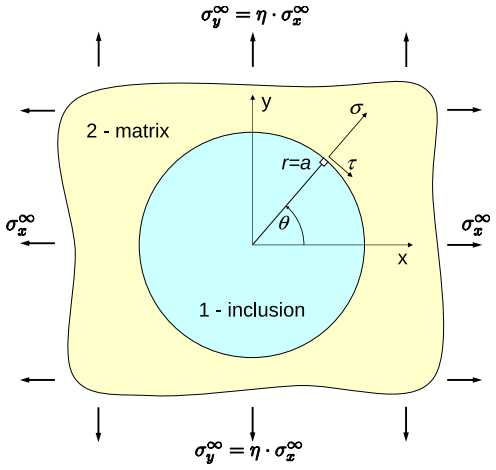

Figure 1: The inclusion problem configuration.

An analytic solution for stresses in this problem was deduced by Goodier (1933). As was shown by

Hardiman (1954) the stresses inside the inclusion are constant. Following Mantič (2009), these inclusion stresses are rewritten in terms of the Dundurs bimaterial constants α and β (Dundurs (1967, 1969)) as follows:

$$\begin{pmatrix} \sigma_x^{(1)} & \sigma_{xy}^{(1)} \\ \sigma_{xy}^{(1)} & \sigma_y^{(1)} \end{pmatrix} = \sigma_x^\infty \begin{pmatrix} k & 0 \\ 0 & k-m \end{pmatrix} + \sigma_y^\infty \begin{pmatrix} k-m & 0 \\ 0 & k \end{pmatrix}, \tag{1}$$

where

$$k(\alpha,\beta) = \frac{1}{2}\frac{1+\alpha}{1+\beta}\frac{2+\alpha-\beta}{1+\alpha-2\beta} \quad \text{and} \quad m(\alpha,\beta) = \frac{1+\alpha}{1+\beta}, \tag{2}$$

and the Dundurs bimaterial constants are defined as

$$\alpha = \frac{\mu_1(\kappa_2+1)-\mu_2(\kappa_1+1)}{\mu_1(\kappa_2+1)+\mu_2(\kappa_1+1)} \quad \text{and} \quad \beta = \frac{\mu_1(\kappa_2-1)-\mu_2(\kappa_1-1)}{\mu_1(\kappa_2+1)+\mu_2(\kappa_1+1)}, \tag{3}$$

with $\mu_k = E_k/(2(1+\nu_k))$ and $\kappa_k = 3-4\nu_k$, E_k and ν_k denoting the Young's modulus and Poisson's ratio, respectively. It can be shown that $0 \le k \le 5/3$ and $0 \le m \le 2$.

Let a dimensionless load-biaxiality parameter η be defined as the ratio of remote stresses

$$\eta = \frac{\sigma_y^\infty}{\sigma_x^\infty}. \tag{4}$$

Then, normal and tangential tractions, σ and τ, acting along the interface ($r=a$) can be expressed as a function of the polar angle θ (see Figure 1) and the parameter η as

$$\frac{\sigma(\theta)}{\sigma_x^\infty} = \frac{\sigma_r(\theta)}{\sigma_x^\infty} = k + (k-m)\eta - (1-\eta)m\sin^2\theta, \tag{5a}$$

$$\frac{\tau(\theta)}{\sigma_x^\infty} = \frac{-\sigma_{r\theta}(\theta)}{\sigma_x^\infty} = (1-\eta)\sin\theta\cos\theta. \tag{5b}$$

In view of the problem symmetry only angles $0° \le \theta \le 90°$ will be considered for the sake of simplicity.

In the following and without loss of generality it will be assumed that $\sigma_x^\infty > 0$ and $\sigma_x^\infty \ge \sigma_y^\infty$, i.e. $\eta \le 1$. The derivative of $\sigma(\theta)$ evaluated from (5a),

$$\frac{\partial \frac{\sigma(\theta)}{\sigma_x^\infty}}{\partial\theta} = (\eta-1)m\sin(2\theta). \tag{6}$$

This shows that normal traction is a decreasing function of θ for $\theta \in [0°, 90°]$ and any $\eta \le 1$. According to this and the expression in (5a), $\sigma(\theta)$ achieves its maximum value at $\theta = 0°$:

$$\sigma_{\max} = \sigma(\theta = 0°) = \sigma_x^\infty \cdot k + \sigma_y^\infty \cdot (k-m). \tag{7}$$

Note that k and $k-m$ represent, respectively, the relative contribution of remote stresses σ_x^∞ and σ_y^∞ to this maximum value of $\sigma(\theta)$.

Following (5a) and (7), the influence of σ_y^∞ on the normal stresses $\sigma(\theta)$ is determined by the ratio k/m. In particular, tension $\sigma(\theta = 0°) > 0$ is generated by a remote compression $\sigma_y^\infty < 0$ (tension $\sigma_y^\infty > 0$) for $k/m < 1$ ($k/m > 1$), assuming small$\sigma_x^\infty \gtrsim 0$.

Recalling that $\sigma_x^\infty > 0$, the semiangle θ_0 for which the interface normal tractions vanish is given from (5a) by

$$\theta_0(\eta;\alpha,\beta) = \arcsin\sqrt{\frac{\frac{k}{m} + \left(\frac{k}{m}-1\right)\eta}{1-\eta}}. \tag{8}$$

According to this expression and the analysis in Appendix A, the angle $\theta_0 \in [0°, 90°]$ does not exist for

Table 1: Examples of isotropic bimaterials constants (1, inclusion; 2, matrix)

Bimaterial	E_1(GPa)	ν_1	E_2(GPa)	ν_2
Glass/epoxy	70.8	0.22	2.79	0.33
Carbon/epoxy	13.0	0.20	2.79	0.33

	α	β	ε	E^* (GPa)
Glass/epoxy	0.919	0.229	-0.074	6.01
Carbon/epoxy	0.624	0.136	-0.044	5.09

	k	m	k/m	$\theta_\eta(^\circ)$	η_0
Glass/epoxy	1.44	1.56	0.9205	16.3	0.086
Carbon/epoxy	1.32	1.43	0.9200	16.4	0.087

all the considered values of $\eta \in (-\infty, 1]$ and all admissible values of $\frac{k}{m} \in [3/4, +\infty)$, see Mantič (2009).

The condition of vanishing derivative of (5a) with respect to η gives the angle θ_η for which the interface normal traction is independent of η,

$$\theta_\eta\,(\alpha, \beta) = \arccos\sqrt{\frac{k}{m}} = 90^\circ - \theta_0(\eta = 0). \tag{9}$$

This expression makes sense only if $k \leq m$. Then, θ_η divides the interface sector $0 \leq \theta \leq 90^\circ$ into two regions. In the first region ($\theta < \theta_\eta$) where $\frac{\partial \sigma}{\partial \eta} < 0$, σ decreases with increasing the remote secondary load σ_y^∞. On the contrary, in the second region ($\theta > \theta_\eta$) where $\frac{\partial \sigma}{\partial \eta} > 0$, σ increases with increasing the remote secondary load σ_y^∞. Hence, θ_η is a key angle to evaluate the influence of load biaxiality.

The values of the above defined and used constants characterizing the interface traction distribution for two typical fibre reinforced composites are presented in Table 1. The glass/epoxy bimaterial will be used as an example in the present work.

Plots of normal tractions distributions along the interface obtained from (5a) for glass/epoxy are shown in Figure 2.

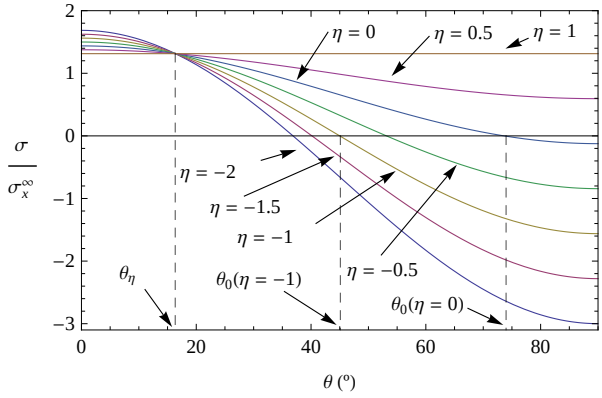

Figure 2: Distribution of the normal tractions along the interface for several values of η and glass/epoxy.

3. The solution for a crack at the interface of a single inclusion under a remote biaxial transverse load

Energy based fracture criteria consider a cracked configuration. Hence the aim of this section is to analyse the problem of a partial debond at the fibre-matrix interface. Under certain assumptions, a classical elastic solution particularized for the present problem provides closed form expressions for a fracture mode mixity and the energy release rate, their dependence on the key problem parameters being pointed out.

Consider now the problem configuration from the previous section altered by the presence of a crack at the interface. In view of the fact that the maximum of $\sigma(\theta)$ is achieved at $\theta = 0°$, see (6), it will be assumed that this crack is symmetrically situated with respect to the x-axis, with a semidebond angle $\theta_d \geq 0$ and an infinite length in the z-axis direction, see Figure 3.

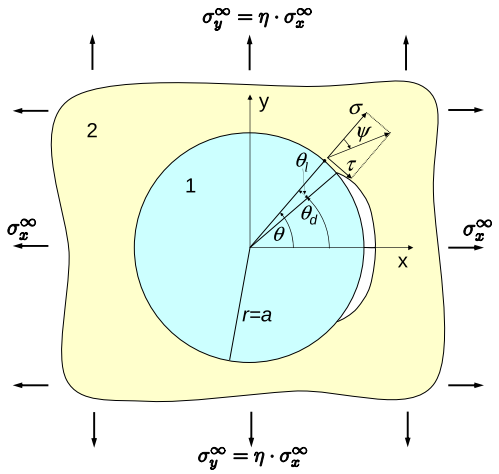

Figure 3: The interface crack problem configuration.

A more general problem has been analytically studied by Toya (1974) and several other authors using the open model of interface cracks. As will be seen later on, the validity of the analytic solutions based on the open model is limited and, thus, computational methods should sometimes be used employing the contact model of interface cracks, see París et al. (2007) for a review.

The interface tractions at a point placed ahead of the crack tip at the polar angle $\theta = \theta_d + \theta_l$, $\theta_l > 0$, see Figure 3, can be expressed by particularizing Toya's solution for stresses[1] and rewriting it in terms of the Dundurs parameters,

$$\sigma(\theta, \theta_d, \eta, \beta) - i\tau(\theta, \theta_d, \eta, \beta) = -\frac{\sigma_x^\infty}{2}\frac{1-\alpha}{1-\beta}\chi(\theta, \theta_d, \beta)p(\theta, \theta_d, \eta, \beta), \tag{10}$$

where $\chi(\theta, \theta_d, \beta)$ and $p(\theta, \theta_d, \eta, \beta)$ are defined in Appendix B). It should be noticed that the tractions along the interface are independent of the inclusion radius a. Ratio of the interface shear and normal tractions ahead the crack tip at a small reference length (either geometry or material based) gives a measure of fracture mode mixity of an interface crack. Thus, the angle ψ at a reference angle θ_l, measured from the crack tip (see Mantič (2009) for the discussion about this reference angle for a similar problem), is defined as:

$$\tan\psi(\theta_d; \theta_l, \eta, \varepsilon) = \frac{\tau(\theta_d + \theta_l)}{\sigma(\theta_d + \theta_l)}. \tag{11}$$

This angle will be used as a suitable measure of the fracture mode mixity. Figure 4 shows the evolution of $\psi(\theta_d)$ for different values of the load-biaxiality parameter η.

The ERR of the interface crack propagating at its upper crack tip at an angle θ_d can be expressed, rewriting Toya's expression as previously, by

$$G(\theta_d; \sigma_x^\infty, \sigma_y^\infty; a; E^*, \alpha, \beta) = \frac{(\sigma_x^\infty)^2 a}{E^*}\hat{G}(\theta_d; \eta; \alpha, \beta), \tag{12}$$

[1]The following values of the parameters used by Toya: $\phi = 0$ and $\varepsilon_\infty = 0$ are taken.

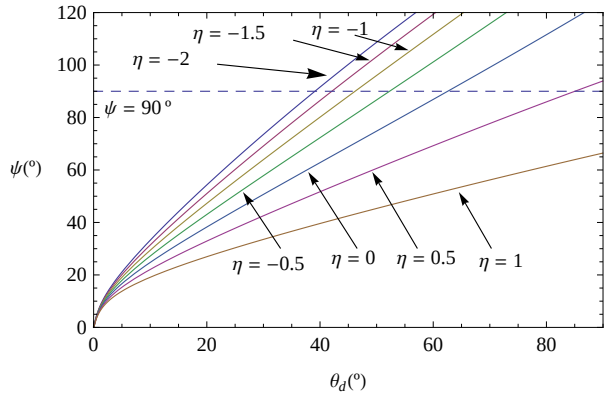

Figure 4: Examples of the evolution of the fracture mode mixity angle ψ (obtained from Toya's solution of the open model of interfacial cracks) taking $\theta_l = 0.1°$, for different values of η and glass/epoxy.

where E^* is the harmonic mean of the effective elasticity moduli

$$\frac{1}{E^*} = \frac{1}{2}\left(\frac{1-\nu_1^2}{E_1} + \frac{1-\nu_2^2}{E_2}\right) \tag{13}$$

and $\hat{G}$ is a dimensionless normalized ERR whose expression is presented in Appendix C. According to expression (12), the ERR varies linearly with the ratio a/E^* and quadratically with the remote load σ_x^∞.

Figure 5 shows the evolution of the normalized ERR $\hat{G}(\theta_d)$, and also of its asymptotes for $\theta_d \approx 0°$ given by (D.1), for different values of the load-biaxiality parameter η, see Appendix D. Validity of these plots is limited by the validity of the open model of interface cracks. Notice, in relation to Figure 4, that compressions ahead of the crack tip correspond to $|\psi| > 90°$ and can become relevant for $\eta < 0$. These compressions may have associated a relevant overlapping of crack faces close to the crack tip. This is not physically admissible, so it may invalidate Toya's solution for some values of θ_d and η.

Due to the above mentioned overlapping, an additional fictitious term, corresponding in some sense to Mode I, appears in the computation of the ERR, causing some overestimation of $\hat{G}$. This overestimation can be studied by using the relation between the ERR based fracture mode mixity and the stress based fracture mixity according to Mantič and París (2004). This relation allows partitioning $\hat{G}$ into two components $\hat{G}(\theta_d) = \hat{G}_I(\theta_d, \delta\theta) + \hat{G}_{II}(\theta_d, \delta\theta)$, for a given virtual-crack-step angle $\delta\theta$, as shown in Appendix E, leading to,

$$\hat{G}_{I,II}(\theta_d, \delta\theta) = \frac{1}{2}\hat{G}(\theta_d)(1 \pm F(\varepsilon)\cos(2(\psi(\theta_d, \theta_l) + \psi_0(\delta\theta/\theta_l, \varepsilon))), \tag{14}$$

where θ_l is the reference angle for ψ (11) and the oscillation index ε is given in terms of β in (B.4).

Figure 6 shows the individual components of the ERR corresponding to a small virtual-crack-step angle $\delta\theta = 0.5°$. These plots allow to clarify the range of validity of Toya's expression of ERR for larger values of θ_d and different values of η. Decreasing values of η decreases the range of the values of θ_d, where Toya's expression of ERR is valid. This figure also confirms that the cause of the strongly increase of $\hat{G}$ for large values of θ_d and $\eta < 0$ is associated to a fictitious contribution of $\hat{G}_I$ due to a large overlapping.

In order to clarify the influence of the remote secondary load σ_y^∞ on the values of $\hat{G}$, it is useful to study the variation of the derivative of $\hat{G}$ (D.1) with respect to the load-biaxiality parameter η at $\theta_d \cong 0°$,

$$\left.\frac{\mathrm{d}^2\hat{G}}{\mathrm{d}\eta\mathrm{d}\theta_d}\right|_{\theta_d=0} = \frac{2\pi(k-m)\left(k+(k-m)\eta\right)\left(1+4\varepsilon^2\right)}{\cosh\left(\pi\varepsilon\right)}. \tag{15}$$

This expression shows again the importance of the parameter k/m. In fact, the sign of the variation of

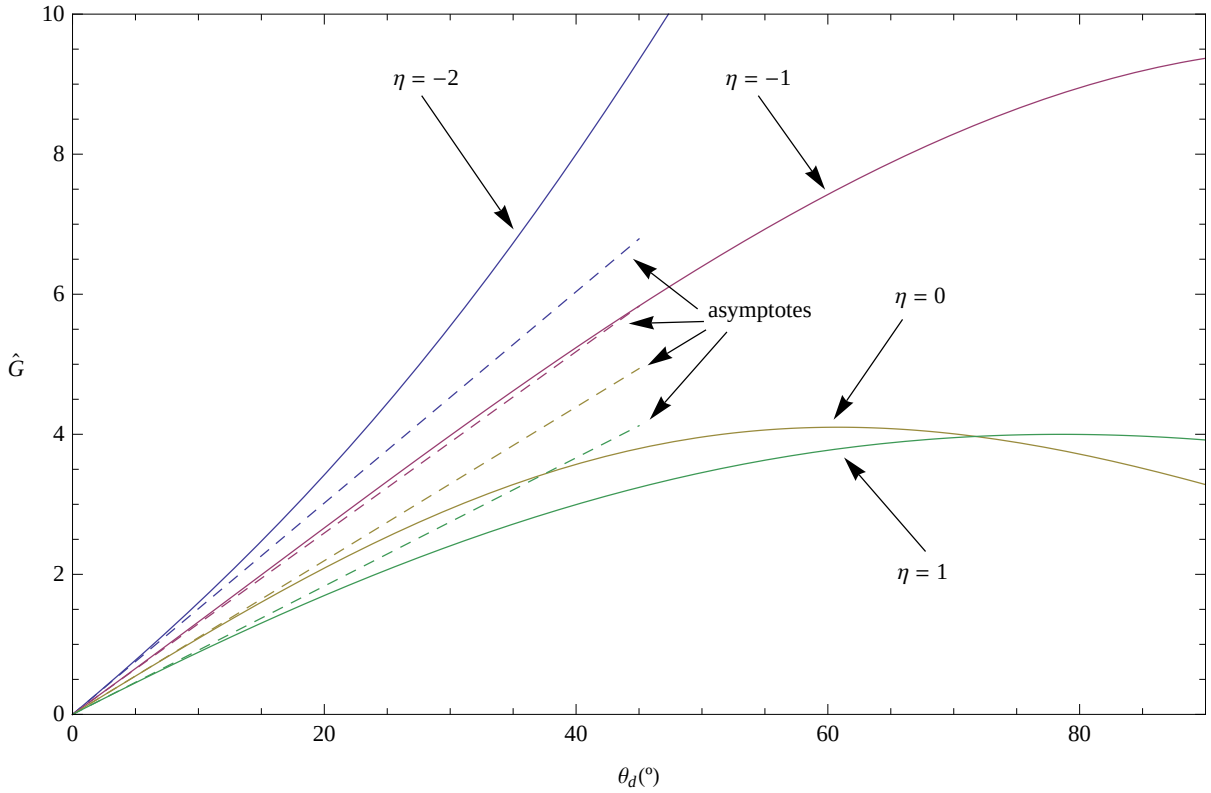

Figure 5: Examples of the normalized ERR (obtained from Toya's solution of the open model of interfacial cracks) and its asymptotes for different values of η and glass/epoxy.

the asymptotic slope of $\hat{G}$ at $\theta_d \cong 0^\circ$ with η is directly characterized by

$$\operatorname{sign} \left. \frac{\mathrm{d}^2 \hat{G}}{\mathrm{d}\eta \mathrm{d}\theta_d} \right|_{\theta_d=0} = \operatorname{sign} \left(\frac{k}{m} - 1 \right) \left(\frac{k}{m} + \left(\frac{k}{m} - 1 \right) \eta \right). \tag{16}$$

According to (16), a change of monotonicity of the asymptotic slope of $\hat{G}$ at $\theta_d \cong 0^\circ$ occurs for (see Appendix A)

$$\eta = \frac{\frac{k}{m}}{1 - \frac{k}{m}} = \frac{1}{\eta_0}. \tag{17}$$

Thus, the sign of derivative in (15), cf. (16), for $\frac{k}{m} > 1$ is positive for $1/\eta_0 < \eta \leq 1$ and negative for $\eta < 1/\eta_0$, whereas for $\frac{k}{m} < 1$ it is negative for all the values of $\eta \leq 1$. Consequently, for bimaterials with $\frac{k}{m} < 1$, a remote secondary tension $\sigma_y^\infty > 0$ will hinder the crack onset from the energetic approach point of view, while a secondary compression $\sigma_y^\infty < 0$ will facilitate it.

4. Interface crack onset at a single inclusion under a remote biaxial transverse load

The approach developed by Leguillon (2002) in the framework of the Finite Fracture Mechanics will be used to predict the crack onset, in a similar way as done in Mantič (2009) for remote uniaxial load. The key idea of this approach is to combine a stress and an energy criterion to predict the critical load originating crack onset and the crack length at the onset. The reason for applying the coupled criterion is that it is not possible to obtain a solution of the crack onset problem by applying each criterion individually without some extra assumptions due to the following reasons:

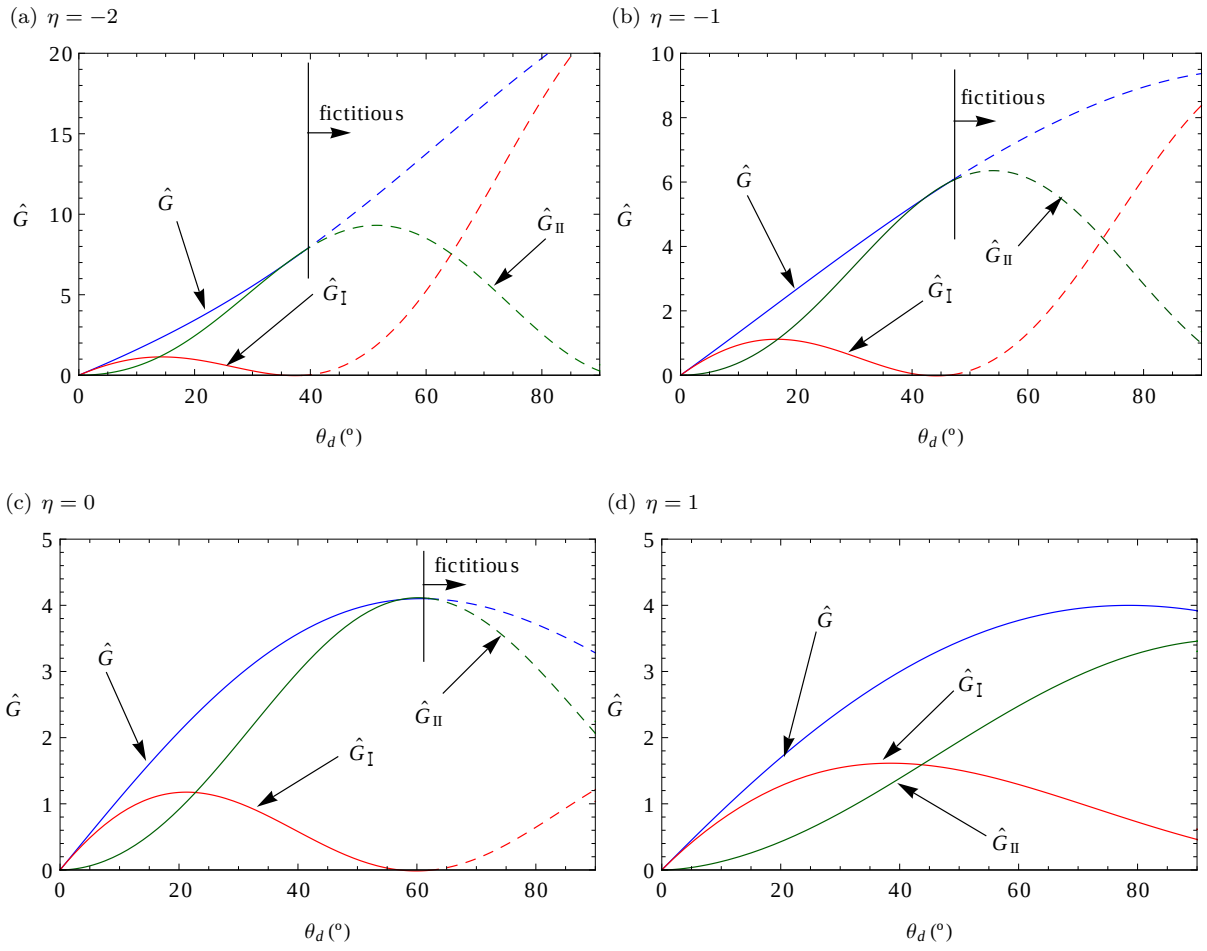

Figure 6: Plots of the individual components of the ERR associated to $\delta\theta = 0.5^{\circ}$ for different values of the load-biaxiality parameter η and glass/epoxy. (a) $\eta = -2$. (b) $\eta = -1$. (c) $\eta = 0$. (d) $\eta = 1$.

- A stress criterion can determine the minimal load but it cannot determine the size of the crack originated at the onset.
- An application of the infinitesimal Griffith criterion requires an existing crack to obtain a value of G different from 0 in order to fulfill the condition $G \geq G_c > 0$.

However, coupling both criteria and releasing the Griffith condition of infinitesimal crack growth by allowing finite increments of crack advancing, permits to obtain the length of the crack originated and the critical load required for the onset.

In view of the remote tension σ_x^{∞} dominating the crack onset and the problem symmetry with respect to the x-axis, onset of a crack situated as shown in Figure 3 will be assumed in agreement with experimental observations. Reasons why, in spite of the symmetry with respect to the y-axis, only one crack appears, resulting in an asymmetric configuration after the crack onset will be discussed in a forthcoming paper by García et al. (2012).

First, in Subsection 4.1, the stress criterion is presented and applied to the stress state analysed in Section 2. Second, a condition imposed by the incremental energy criterion is obtained in Subsection 4.2 with the aid of the analysis introduced in Section 3. Then, both conditions are combined in Subsection 4.3 leading to the prediction of the critical load and semiangle. Finally, the post-crack-onset evolution and the applicability of the open model of interface cracks in the present problem are discussed in Subsections 4.4 and 4.5, respectively.

4.1. Stress criterion

A stress criterion is usually invoked if no crack exists *a priori*. The present stress criterion is based on the idea of the existence of an interface tensile-strength σ_c, defined as the maximum tension that the interface can sustain. Thus, in the present problem, the inclusion-matrix interface can break at the points defined by an angle θ where,

$$\sigma(\theta) \geq \sigma_c, \tag{18}$$

defining a tensile criterion. According to Figure A.1 and Section 2, this criterion cannot be fulfilled for $\eta \leq 1/\eta_0$ and $k/m > 1$ because the whole interface is under compression and no crack onset can be predicted following the stress criterion. Hence, in the following analysis, it will be assumed that either $\eta > 1/\eta_0$ or $k/m \leq 1$.

Then, combining (18) and (5a), the stress criterion can be expressed as

$$\frac{\sigma_x^\infty}{\sigma_c} \geq \frac{1}{k + (k-m)\eta - (1-\eta)m\sin^2\theta} = s(\theta, \eta, \alpha, \beta). \tag{19}$$

Assuming a sufficiently large remote loading, given by (19) for $\theta = 0°$,

$$\frac{\sigma_x^\infty}{\sigma_c} \geq \min_\theta s(\theta, \eta) = s(0°, \eta) = \frac{1}{k + (k-m)\eta} > 0, \tag{20}$$

an angle $\theta_c^\sigma \in [0°, 90°]$ can be defined by $\sigma(\theta_c^\sigma) = \sigma_c$. Then, due to the decreasing character of $\sigma(\theta)$ (see (6) and discussion in Section 2), condition (18) is verified for all $\theta \in [0°, \theta_c^\sigma]$,

$$\theta_c^\sigma = \arcsin\sqrt{\frac{k + (k-m)\eta - \frac{\sigma_c}{\sigma_x^\infty}}{(1-\eta)m}}, \tag{21}$$

According to a discussion in Section 2, for a given value of η an angle θ_0 (8) may exist where the traction is zero. Then, condition (19) leads to an infinite load for $\theta = \theta_0$, which is an upper limit for the values of θ_c^σ,

$$\theta_c^\sigma < \theta_0(\eta; \alpha, \beta) \tag{22}$$

Then, combining all the conditions related to the stress criterion, the maximum angle of a debond and the function s are defined in a rigorous manner suitable for computational proposes in Appendix F.

Figure 7 shows a representation of the stress criterion for glass/epoxy as defined in Table 1 for different values of η. As predicted, all the curves of the stress criterion are increasing. Thus, for a load (values of σ_x^∞/σ_c and η) two zones can be defined in this diagram if θ_c^σ exists, a zone where a debond is possible $[0°, \theta_c^\sigma]$, and another where it is not possible $(\theta_c^\sigma, 180°]$.

Note that an angle θ_η (see Figure 7) can be defined where the stress criterion is independent of the remote secondary load σ_y^∞ as demonstrated in Section 2. This semiangle separates the interface into two regions, a region ($\theta < \theta_\eta$) where a secondary compression $\sigma_y^\infty < 0$ facilitates a debond onset and another region ($\theta > \theta_\eta$) where it hinders a debond.

Finally it should be noticed that the stress criterion is not sufficient to uniquely characterize the debond onset, as it provides only one inequality for two unknowns, the critical remote load and debond angle after the onset.

4.2. Incremental Energy criterion

An incremental Griffith criterion is used here with the aid of expressions developed in Section 3. First, an energy balance for the onset of an interface crack of a finite length is introduced and its different terms are particularized for this problem and analysed. Finally, a condition for the minimum load originating an energetically allowed fibre-matrix debond is deduced by means of a dimensionless function of the crack length representing the ratio of the dissipated to the released energy.

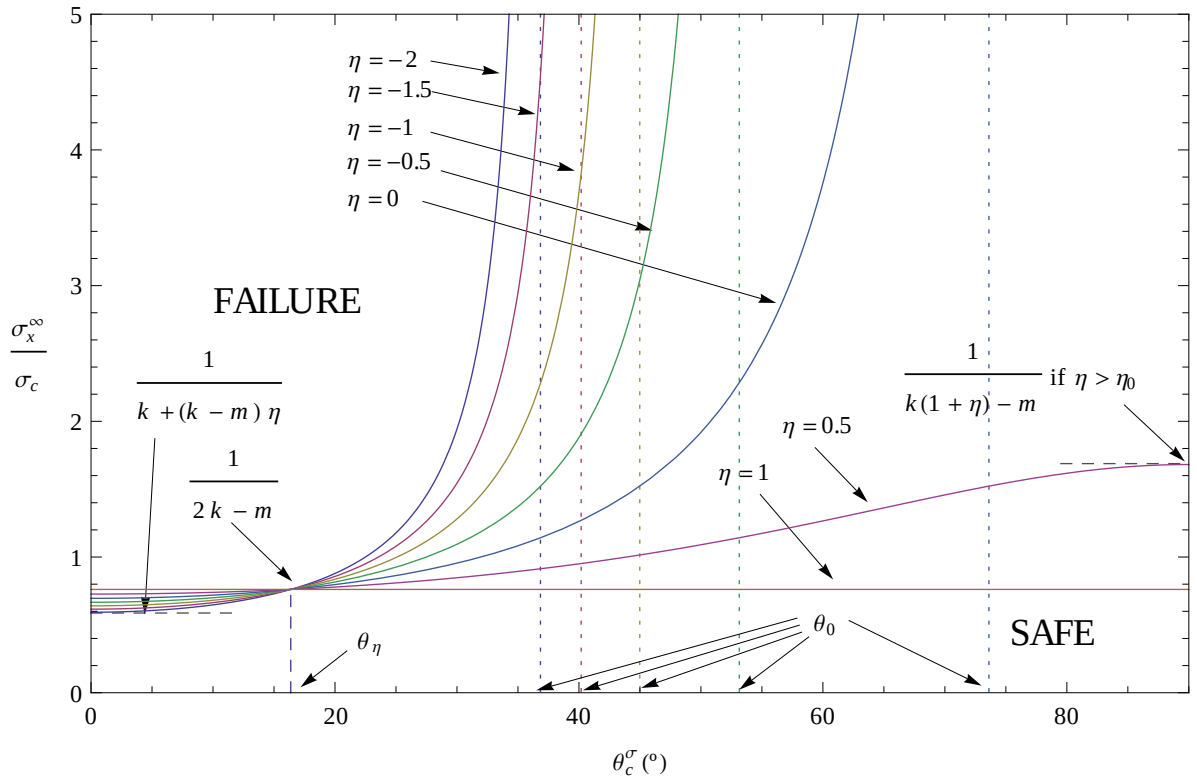

Figure 7: Graphical representation of the stress criterion for different values of η and glass/epoxy.

Similarly as in Mantič (2009), the energy balance can be written as

$$\Delta\Pi + \Delta E_k + 2\int_0^{\Delta\theta} G_c(\theta_d) a \mathrm{d}\theta_d = 0, \tag{23}$$

where $\Delta\Pi$ is the change in the potential energy between the states prior to and after the onset of the finite length crack, ΔE_k is the change in the kinetic energy of the body, G_c is the interface fracture toughness (called also fracture energy) and $\Delta\theta$ is the semiangle of the finite crack originated at onset. Note that heat transfer and other types of dissipation have been neglected.

Interface fracture toughness G_c is considered to be dependent on the semidebond angle θ_d as explained in the following. According to Hutchinson and Suo (1992), see also Mantič et al. (2006) and further references therein, the variation of fracture toughness of an interface crack depends on the fracture mode mixity. Fracture mode mixity of the crack growing along the inclusion-matrix interface can be characterized by the phase angle ψ defined in (11), writing $G_c(\theta_d) = G_c(\psi(\theta_d, \eta))$. The following phenomenological law proposed by Hutchinson and Suo (1992):

$$G_c(G_{1c}, \psi, \lambda) = G_{1c}\hat{G}_c(\psi, \lambda) = G_{1c}\left(1 + \tan^2\left[(1-\lambda)\psi\right]\right), \tag{24}$$

will be used in the present analysis. G_{1c} is considered as the fracture Mode I toughness, λ is a fracture mode-sensitivity parameter, typical range $0.2 \leq \lambda \leq 0.35$ being characteristic of moderately strong fracture mode dependance, $\hat{G}_c$ is a dimensionless normalized fracture toughness function.

Figure 8 shows the evolution of the interface fracture toughness as a function of θ_d, taking $\theta_l = 0.1°$ and $\lambda = 0.3$, for different values of the load-biaxiality parameter η. Fracture toughness plots for negative values of η have vertical asymptotes at moderate values of θ_d. This is due to the effect of the secondary compression $\sigma_y^\infty < 0$ on the fracture mode mixity increasing the participation of the fracture Mode II.

The energetic balance (23) can be rewritten, in view of the above analysis and assuming the production

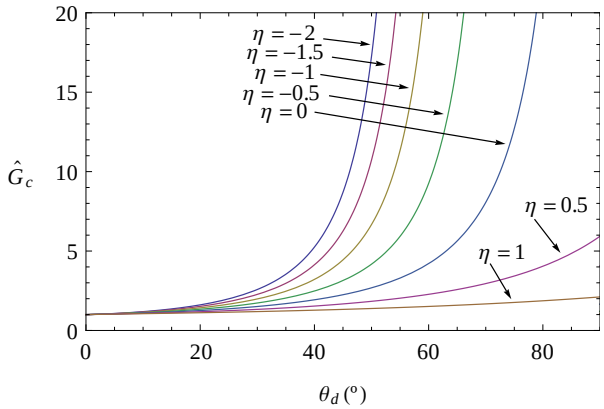

Figure 8: Examples of the normalized interface fracture toughness evolution $\hat{G}_c(\psi(\theta_d, \eta))$ for different values of η, taking $\lambda = 0.3$, $\theta_l = 0.1°$ and glass/epoxy.

of kinetic energy because of the quasi-static initial state ($\Delta E_k > 0$), as

$$-\Delta\Pi \geq \int_0^{\Delta\theta} G_c(\psi(\theta_d, \eta))\mathrm{d}\theta_d. \tag{25}$$

Employing the relation between the differential ERR and the derivative of the potential energy with respect to the crack length $G = -\frac{\mathrm{d}\Pi}{\mathrm{d}(2a\theta_d)}$, this inequality leads to the energetic condition

$$\int_0^{\Delta\theta} G(\theta_d; \sigma_x^\infty, \eta; a; E^*, \alpha, \beta)\mathrm{d}\theta_d \geq \int_0^{\Delta\theta} G_c(G_{1c}, \psi(\theta_d, \eta))\mathrm{d}\theta_d. \tag{26}$$

Inasmuch as $G(0°) = 0$ and $G_c(\psi(0°, \eta)) > 0$, there is no solution of (26) for values of $\Delta\theta$ lower than a minimum semiangle θ. Thus, the energy criterion imposes, at least, a lower limit for the length of the originated crack.

By substituting G from (12) and G_c from (24) into (26), the expression of the incremental energy criterion takes the form

$$\frac{(\sigma_x^\infty)^2\, a}{G_{1c} E^*} \geq g\left(\Delta\theta, \eta\right), \tag{27}$$

where

$$g(\Delta\theta, \eta; \alpha, \beta; \lambda, \theta_l) = \frac{\int_0^{\Delta\theta} \hat{G}_c\left(\psi(\theta_d, \eta)\right) \mathrm{d}\theta_d}{\int_0^{\Delta\theta} \hat{G}(\theta_d, \eta)\mathrm{d}\theta_d} > 0. \tag{28}$$

Note that, the dimensionless function g is independent of the particular values of the strength and fracture toughness parameters that characterize the interface, except for the model parameters λ and θ_l. It represents the ratio of the dimensionless forms of the incremental dissipated energy to the incremental released energy.

Figure 9 shows the evolution of the dimensionless function g (computed by numerical integration) and its curvilinear asymptote calculated in Appendix D for different values of η and for glass/epoxy defined in Table 1. The function g has a minimum at an angle that will be denoted as $\theta^E_{\min}(\eta; \alpha, \beta; \lambda, \theta_l) > 0$. The existence of this minimum can be deduced from the behaviour of the functions $\hat{G}_c$ and $\hat{G}$.

Taking into account that $g(\Delta\theta)$ is a decreasing function for $\Delta\theta < \theta^E_{\min}$, for a sufficiently large σ_x^∞, there exists a lower limit $\theta_c^E \leq \theta^E_{\min}$ for the semiangle $\Delta\theta$ of energetically allowed debonds, defined by the equality in (27):

$$\theta_c^E(\sigma_x^\infty, \eta, G_{1c}; a; E^*, \alpha, \beta; \lambda, \theta_l) \leq \Delta\theta. \tag{29}$$

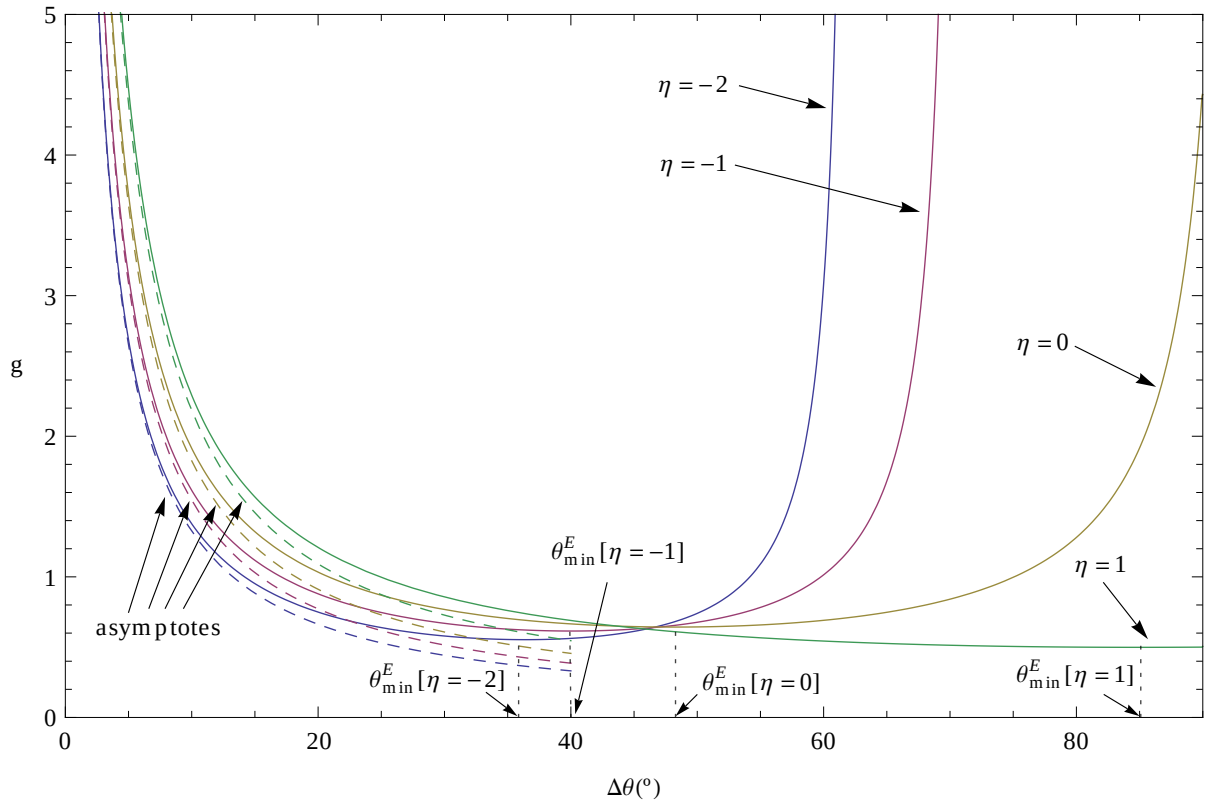

Figure 9: Universal dimensionless function $g(\Delta\theta, \eta)$, taking $\lambda = 0.3$, $\theta_l = 0.1°$ and glass/epoxy.

In the particular case of $\theta_c^E = \theta_{\min}^E$, according to the analysis carried out in Mantič (2009),

$$\int_0^{\theta_{\min}^E} G(\theta_d, \eta)\mathrm{d}\theta_d = \int_0^{\theta_{\min}^E} G_c(\psi(\theta_d, \eta))\mathrm{d}\theta_d \quad \text{and} \quad G(\theta_{\min}^E, \eta) = G_c(\psi(\theta_{\min}^E, \eta)). \tag{30}$$

Additionally, as demonstrated in Appendix G, it can be shown that,

$$\left.\frac{\mathrm{d}G(\theta_d)}{\mathrm{d}\theta_d}\right|_{\theta_d=\theta_c^E=\theta_{\min}^E} \leq \left.\frac{\mathrm{d}G_c(\psi(\theta_d, \eta))}{\mathrm{d}\theta_d}\right|_{\theta_d=\theta_c^E=\theta_{\min}^E}. \tag{31}$$

Assuming that $-G$ and G_c are strictly convex functions in the range of interest, in fact, strict inequality holds in (31), see Mantič (2009). Notice that, according to Figures 5, 6 and 8, $-G$ is strictly convex for $-1 \leq \eta \leq 1$ whereas G_c is convex in all the situations studied.

The existence of a minimum of g leads to the prediction of a minimum load originating an energetically allowed debond,

$$\sigma_{cx}^{\infty,E} = \sqrt{\frac{G_{1c}E^*}{a} g(\theta_{\min}^E, \eta)}. \tag{32}$$

According to Figure 9, a semiangle θ_η^E exists where the function g is roughly independent of the value of η for the bimaterial considered. For $\Delta\theta < \theta_\eta^E$, the value of g reduces with decreasing σ_y^∞ with respect to a fixed σ_x^∞. However, for $\Delta\theta > \theta_\eta^E$ the effect of σ_y^∞ is inverted. Nevertheless, the value of θ_η^E is somewhat large for the model assumptions. Therefore, in most cases of interest, increasing σ_y^∞ for the same σ_x^∞ increases θ_c^E, the lower limit for $\Delta\theta$ allowed energetically.

4.3. Coupled Stress and Energy Criterion

The above stress and energy conditions are combined here taking into account the different monotony of both criteria: stress criterion is an increasing function, whereas energy criterion is decreasing up to a minimum point. As a consequence of this, two different scenarios, brittle and ductile, are presented depending on the parameters of the problem. Next, an algorithm necessary to solve the problem is described. Then, main results are presented focusing on the influence of the biaxiality on the failure behaviour. Results presented in the following show the secondary transverse load modifies slightly the main critical transverse load for glass/epoxy. For tough configurations, an analytical expression of this dependence is obtained as a function of a bimaterial elastic parameter. A study of this influence as a function of bimaterial parameters is presented, in particular for typical composites and extreme cases.

The stress criterion (F.3) and the incremental energy criterion (27), respectively, essentially impose an upper limit θ_c^σ (F.1) and a lower limit θ_c^E (29) for an initial semidebond angle considering given remote loads. Then, onset of a new crack of a semiangle $\Delta\theta$ is only possible if it verifies:

$$\theta_c^E \leq \Delta\theta \text{ and } \Delta\theta \leq \theta_c^\sigma. \tag{33}$$

Typically the two limits converge when decreasing the value of σ_x^∞ for a fixed η. Nevertheless, there is an exception when $\theta_c^\sigma > \theta_{\min}^E$ for the load $\sigma_{cx}^{\infty,E}$ (32). Therefore, two scenarios are possible as described in the following. Without loss of generality, only configurations where $\tilde{\theta}_0$ (A.4) is defined will be analysed.

In scenario A, both criteria, (F.3) and (27) are fulfilled as equalities. This implies that the curves of both criteria have an intersection for a semiangle of the crack after the onset $\Delta\theta = \theta_c$, called critical semidebond angle, giving the minimum value of σ_{cx}^∞,

$$\theta_c = \theta_c^E = \theta_c^\sigma \leq \theta_{\min}^E. \tag{34}$$

As the function $s(\theta, \eta)$ on the right-hand side of the stress criterion is increasing with θ (strictly increasing up to $\tilde{\theta}_0$), it occurs if

$$\gamma\sqrt{g(\theta_{\min}^E, \eta)} \leq s(\theta_{\min}^E, \eta). \tag{35}$$

where γ is a dimensionless parameter defined as (see Mantič (2009))

$$\gamma = \frac{1}{\sigma_c}\sqrt{\frac{G_{1c}E^*}{a}}. \tag{36}$$

The value of θ_c can be computed by solving the following nonlinear equation:

$$\gamma\sqrt{g(\theta_c, \eta)} = s(\theta_c, \eta). \tag{37}$$

Then, the value of the critical load originating a crack is easily calculated, using the previously obtained value of θ_c, from

$$\frac{1}{\eta}\frac{\sigma_{cy}^\infty}{\sigma_c} = \frac{\sigma_{cx}^\infty}{\sigma_c} = \gamma\sqrt{g(\theta_c, \eta)}. \tag{38}$$

In scenario B, where condition (35) is not fulfilled, the minimum load originating a crack is always associated to

$$\theta_c = \theta_{\min}^E, \tag{39}$$

because of the increasing character of g for $\Delta\theta > \theta_{\min}^E$. Hence,

$$\frac{1}{\eta}\frac{\sigma_{cy}^\infty}{\sigma_c} = \frac{\sigma_{cx}^\infty}{\sigma_c} = \gamma\sqrt{g(\theta_{\min}^E, \eta)}, \tag{40}$$

the interface crack onset being essentially governed by the energy criterion. In fact, $\sigma_{cx}^\infty = \sigma_{cx}^{\infty,E}$.

Let a threshold value of γ be defined from the equality in (35) as

$$\gamma_{\rm th}(\eta;\alpha,\beta;\lambda,\theta_l) = \frac{s(\theta^E_{\rm min},\eta)}{\sqrt{g(\theta^E_{\rm min},\eta)}}. \tag{41}$$

It is easy to see, that $\gamma_{\rm th}$ separates scenario A ($0 < \gamma \le \gamma_{\rm th}$) from scenario B ($\gamma > \gamma_{\rm th}$). If $\theta^E_{\rm min} \ge \theta_0$ then $\gamma_{\rm th} = +\infty$ in view of (F.2), which means that only scenario A is possible.

According to the definition of the two scenarios, the critical values of θ_c, σ^∞_{cx} and σ^∞_{cy} can be computed by the procedure shown in Figure 10.

```
If (k/m > 1 and η > 1/η0) or k/m ≤ 1  then
  Find min_Δθ g(Δθ) =def g(θ^E_min)
  If γ√(g(θ^E_min)) < s(θ^E_min)
     Solve the next equation for Δθ < θ^E_min:
     γ√(g(Δθ)) = s(Δθ)
     θc =the solution Δθ of this equation
  Else
     θc = θ^E_min
  Endif
  Compute the critical load σ^∞_cx by
     σ^∞_cx / σc = γ√(g(θc))
   and σ^∞_cy by
     σ^∞_cy / σc = η · σ^∞_cx / σc
Else
  No debond is possible under the present hypotheses
Endif
End
```

Figure 10: Computational procedure for the evaluation of θ_c, σ^∞_{cx} and σ^∞_{cy}, assuming $\eta \le 1$.

The above defined dimensionless structural parameter γ (36) can be referred to as *stress oriented brittleness number* (see Mantič (2009) and further references therein). The adjective "stress oriented" corresponds to the fact that the critical load (remote stress) is in some sense proportional to this number, see (38) and (40). In fact, in scenario B (with $\gamma > \gamma_{\rm th}$) the critical load is linearly proportional to γ. The brittleness number γ is governing brittle-to-tough transition in the fibre-matrix debond onset, small values of γ corresponding to brittle and large values to tough configurations (cf. Kushch et al. (2011)).

Whereas the values of the critical angle and load in tough configurations, usually associated to scenario B, are simply described by (39) and (40), the asymptotic behaviour of these values in brittle configurations with vanishing values of γ ($\gamma \to 0^+$), associated to scenario A, requires a further analysis.

Looking at equation (37), defining θ_c, for $\gamma \to 0^+$, it holds $g(\theta_c,\eta) \to \infty$ because $s(\theta_c,\eta)$ on the right hand side of (37) is bounded from below by its positive minimum value (20) for a fixed η. Taking into account condition (34) and definition of g in (28), see also Figure 9 and approximation (D.3), it is obtained that

$$\lim_{\gamma\to 0^+} \theta_c = 0^\circ. \tag{42}$$

In the same manner, an asymptotic expression can be extrated as demonstrated in Appendix D.

When evaluating the critical load for $\gamma \to 0^+$, which implies $\theta_c \to 0^+$, the following approximation is obtained, see (20):

$$\frac{\sigma^\infty_{cx}}{\sigma_c} \gtrsim s(0^\circ,\eta) > 0 \quad \text{for} \quad \gamma \to 0^+. \tag{43}$$

Combining this equation with the definition of η in (4), the relation between σ^∞_{cx} and σ^∞_{cy} can be approx-

imated as

$$(k-m)\cdot\frac{\sigma_{cy}^{\infty}}{\sigma_c}+k\cdot\frac{\sigma_{cx}^{\infty}}{\sigma_c}\gtrsim 1 \quad \text{for} \quad \gamma\to 0^{+}. \tag{44}$$

This linear relation between critical stresses is given, in fact, by the stress criterion (F.3) when considered for a small angle $\Delta\theta$.

Figure 11, computed using the computational procedure in Figure 10, presents the effect of the brittleness number γ on the critical semiangle θ_c, the arrest semiangle θ_a (defined later in Section 4.4) and on the critical remote load σ_{cx}^{∞}. This figure is a nice illustration of the above mentioned brittle-to-tough transition in the fibre-matrix debond onset. It can be seen that the behaviour of θ_c and σ_{cx}^{∞} agrees with the above analytic predictions, namely (D.4) with (43) for small and (39) with (40) for large values of γ.

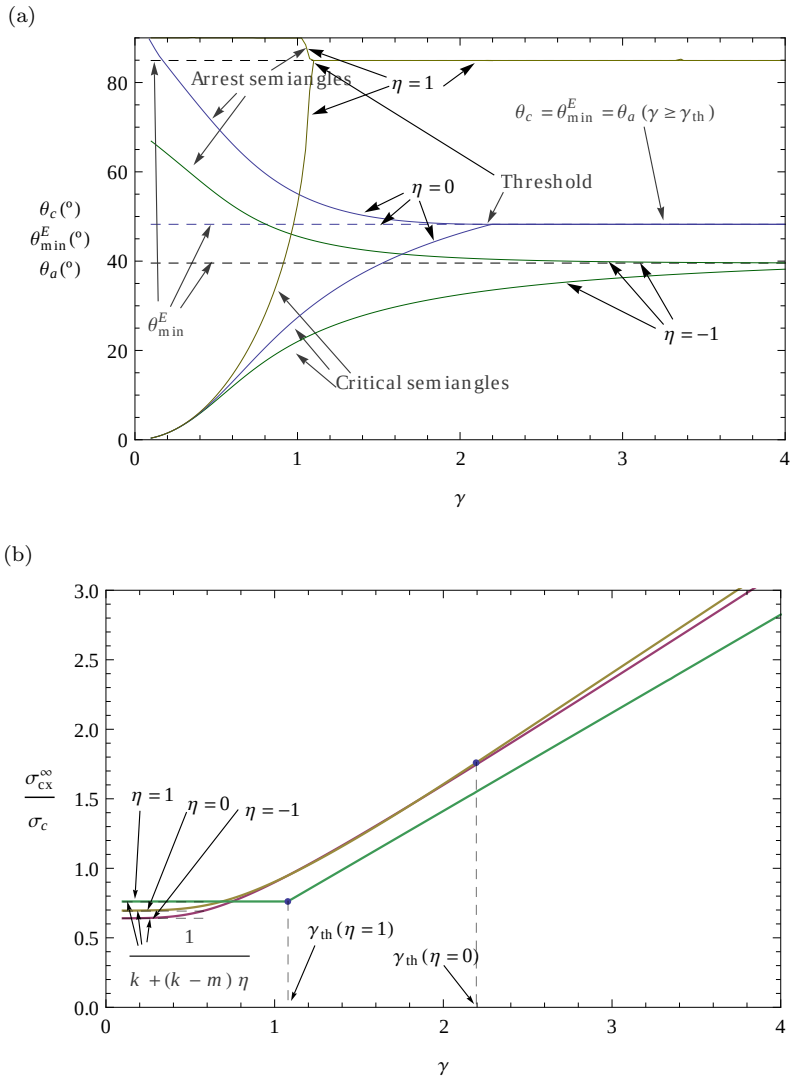

Figure 11: (a) Semiangles θ_c, $\theta_{\min}^{E}$ and θ_a, and (b) Critical remote tension σ_{cx}^{∞} as functions of the brittleness number γ, taking $\lambda = 0.3$, $\theta_l = 0.1°$ and glass/epoxy.

Figure 12 shows the safe regions and failure envelopes in $(\sigma_{cx}^{\infty}, \sigma_{cy}^{\infty})$ plane for glass/epoxy bimaterial computed for different values of γ by applying the procedure described in Figure 10. According to this figure, an increase of remote secondary load σ_{y}^{∞} increases the critical load σ_{cx}^{∞} for sufficiently small values

of γ (recall that $k/m < 1$ and $\eta_0 > 0$ for glass/epoxy). However, a non-monotonic boundary curve of the safe region is observed for greater values of γ in Figure 12. In fact, it is observed that the curve which joins the points with the maximum critical remote load σ_{cx}^{∞} shows that the maximum is situated at $\eta = 1$ just for $\gamma \to 0^+$. For moderate values of γ, the maximum critical remote load σ_{cx}^{∞} corresponds to $\eta < 0$. The reason for this behaviour is clarified in Figure 13 where two situations are explained.

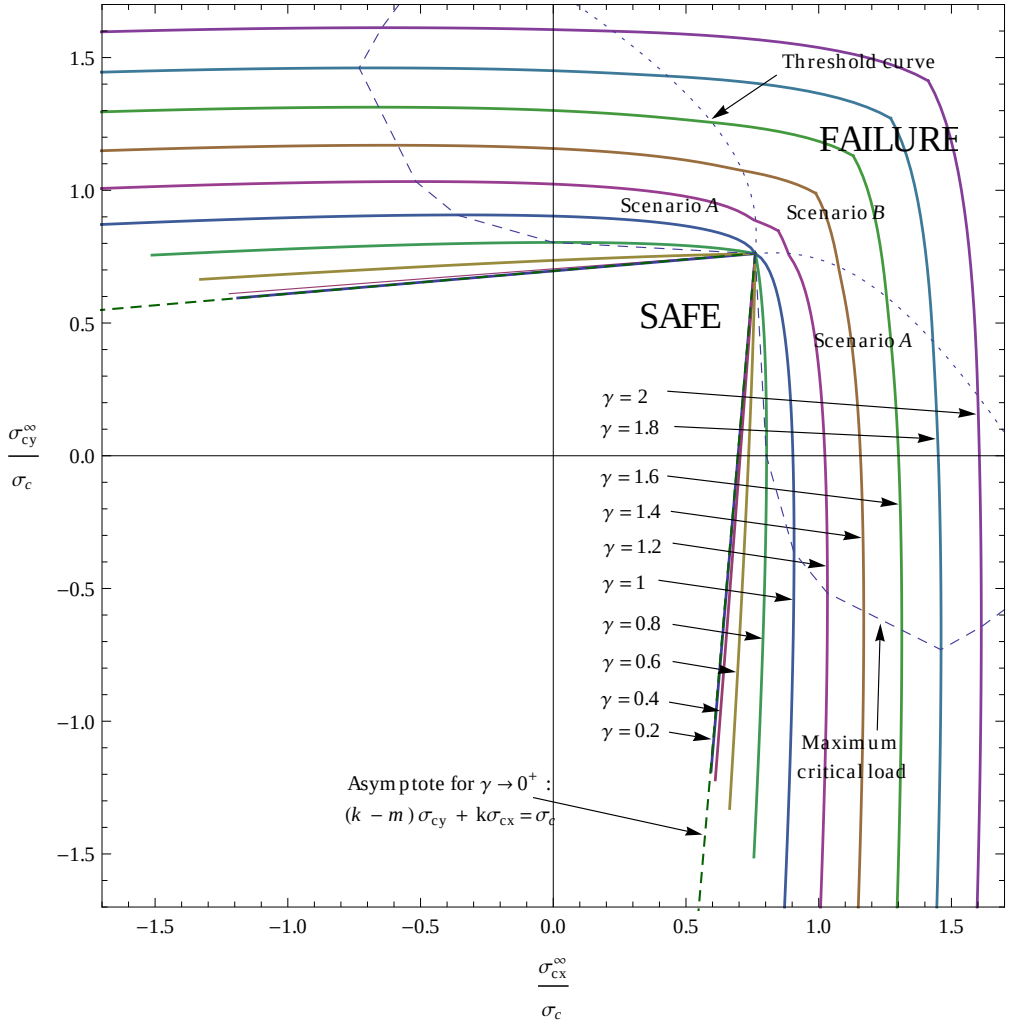

Figure 12: Critical biaxial loads originating a crack for different values of γ, taking $\lambda = 0.3$, $\theta_l = 0.1°$ and glass/epoxy.

In the first case, the value of γ is relatively small, Figure 13(a), which is associated to small values of θ_c, as previously demonstrated. For small values of θ_c, the effect of the secondary load σ_y^{∞} is the same for both the stress criterion and energy criterion curves, both curves descending when η reduces. In the second case, the value of γ is larger, Figure 13(b), and the values of θ_c are greater than θ_η, see (9) and discussion below. Then, for values of γ originating $\theta_c > \theta_\eta$, an increase of the remote secondary load σ_y^{∞} makes less restrictive the stress criterion and more restrictive the energy criterion. Thus, the monotony of the function $\sigma_{cx}^{\infty}(\sigma_{cy}^{\infty})$ can be broken down as observed in Figure 12 for moderate values of γ.

The straight line defined by (44) represents, according to Figure 12, a limit of failure envelope curves for $\gamma \to 0^+$. Note that the failure envelope curves for $\gamma \to 0^+$ in Figure 12 show the most relevant influence of the secondary load σ_y^{∞} on the value of the critical load σ_{cx}^{∞}.

Figure 12 also shows the "threshold curve" which separates scenarios A and B. It is interesting to remark that greater values of γ correspond to a larger range of failure behaviour governed by scenario B. On the contrary, the presence of a remote secondary compression $\sigma_y^{\infty} < 0$ leads to scenario A, for small

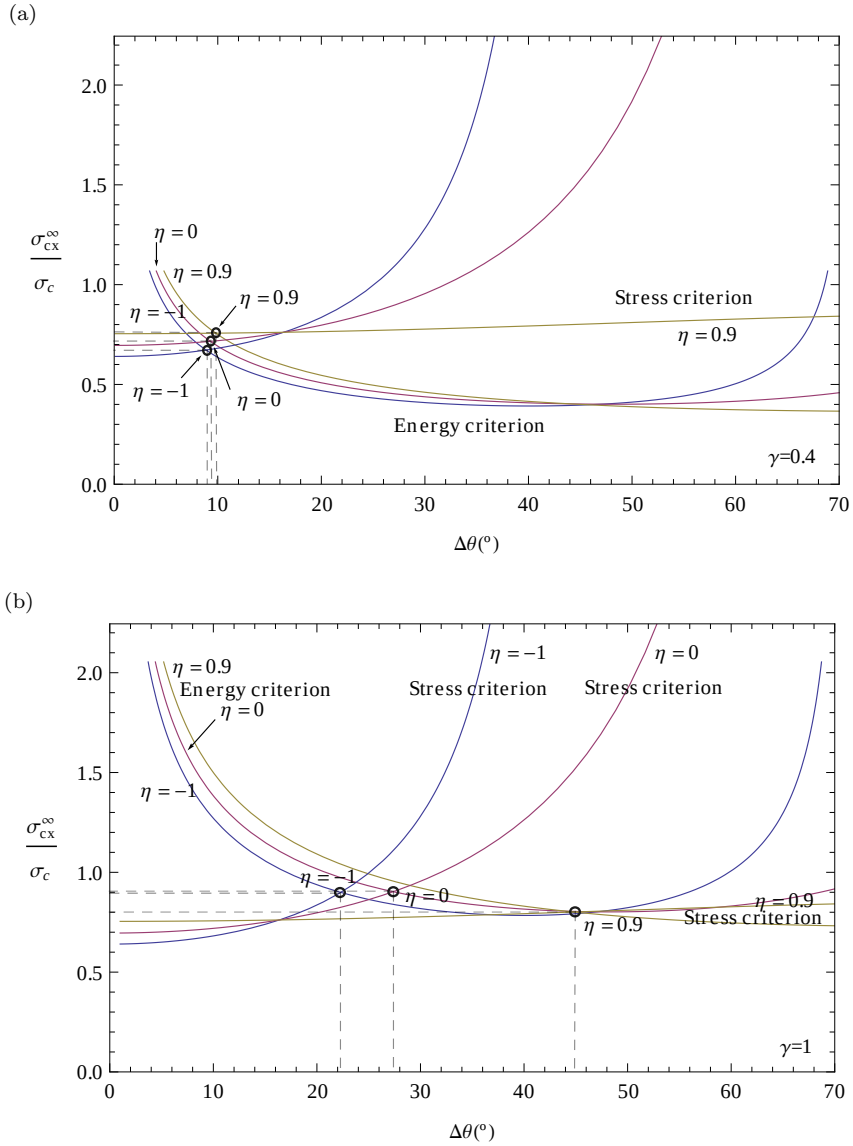

Figure 13: Stress and energy criteria curves, taking $\lambda = 0.3$, $\theta_l = 0.1°$ and glass/epoxy for two different values of γ. (a) $\gamma = 0.4$, (b) $\gamma = 1$

and moderate values of γ.

Figure 14 studies the influence of α and β values on the biaxial safe region for $\gamma \to 0^+$, for selected theoretical (but possible) bimaterials and also for usual composites. From Dundurs' $\alpha - \beta$ parallelogram it is seen that the most common bimaterials have very similar properties in the debond onset problem. A more extensive list of $\alpha - \beta$ values for real bimaterials can be found in Suga et al. (1988) and Schmauder and Meyer (1992).

The safe region in the limit case $\gamma \to 0^+$ is defined by the intersection of the semiplanes including the origin of coordinates and limited by the straight line defined by (44) and the symmetric one with respect to the bisector of the coordinate axes. From (44), the position of the corner point of the safe region ($\eta = 1$) is given by

$$\frac{\sigma_{cx}^{\infty}}{\sigma_c} = \frac{\sigma_{cy}^{\infty}}{\sigma_c} = \frac{1}{2k - m}. \tag{45}$$

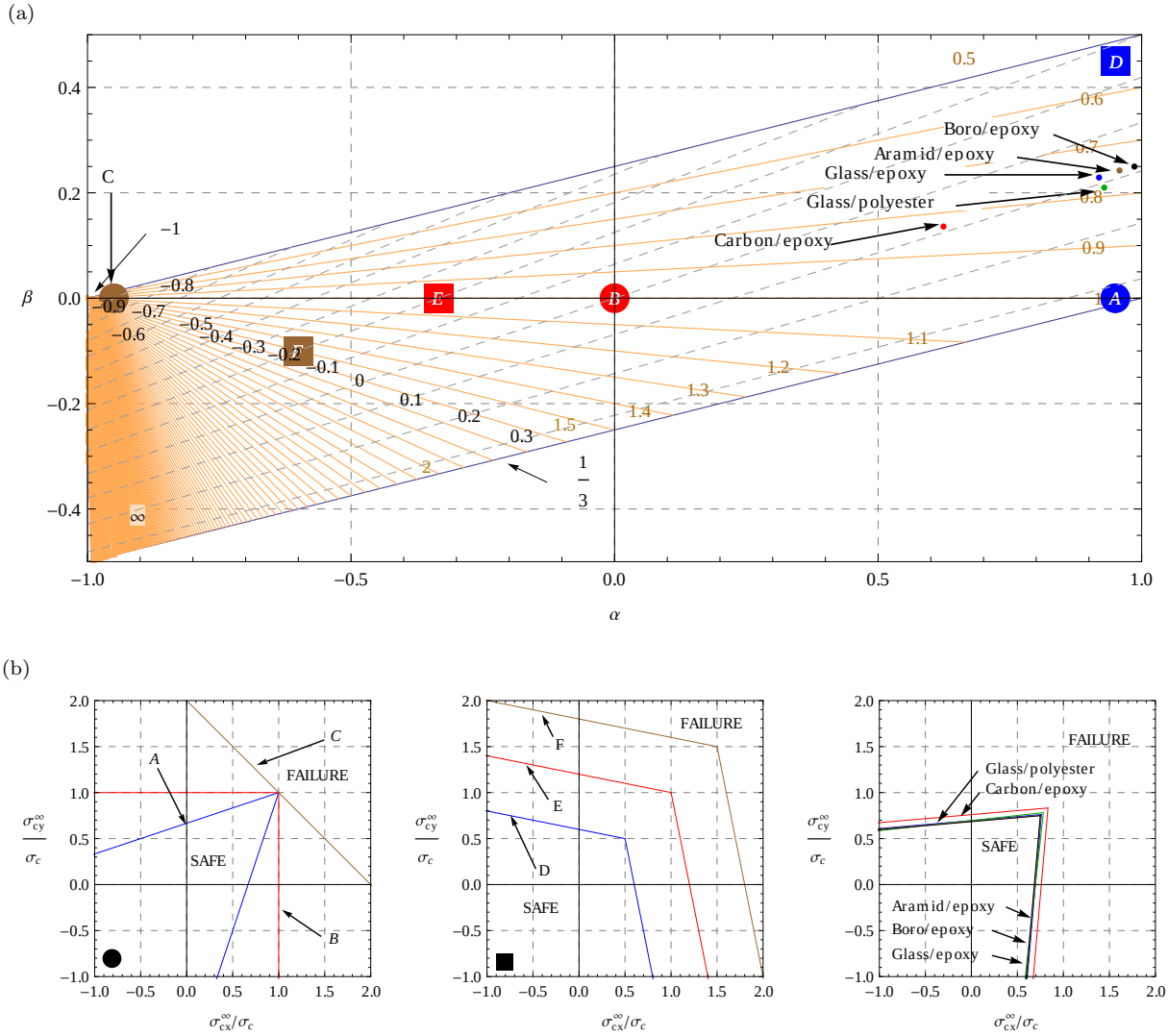

Figure 14: (a) $\alpha - \beta$ diagram for bimaterials in plane strain with isovalue curves for $\gamma \to 0^+$ corresponding to: solid lines with values of $\sigma_{cx}^{\infty}/\sigma_c = \sigma_{cy}^{\infty}/\sigma_c$, and dashed lines with values of $\partial\sigma_{cx}^{\infty}/\partial\sigma_{cy}^{\infty}$. (b) Some biaxial failure envelopes for $\gamma \to 0^+$ for selected points in the $\alpha - \beta$ diagram and usual composites. A: $k/m = 0.75$, B: $k/m = 1$, C: $k/m \to +\infty$, D: $k/m = 1.25$, E: $k/m = 1.25$, F: $k/m = 1.25$, Carbon/epoxy: $k/m = 0.9200$, Glass/polyester: $k/m = 0.9201$, Glass/epoxy: $k/m = 0.9205$, Aramid/epoxy: $k/m = 0.9217$, Boro/epoxy: $k/m = 0.9204$

The slope of the linear relation in (44) characterizes the influence of the secondary load σ_y^{∞} on the critical load σ_{cx}^{∞}. This slope can be expressed as:

$$\lim_{\gamma \to 0^+} \left(\frac{\partial \sigma_{cx}^{\infty}}{\partial \sigma_{cy}^{\infty}} \right) = \eta_0 \tag{46}$$

where η_0 is defined in (A.1) and its range in (A.2), see also Figure A.1. Hence, this slope is only dependent on the elastic bimaterial properties and does not depend on the interface properties. In view of the range of possible values for the slope (A.2), the safe region is always convex, cf. Figure 14(b).

For $k/m < 1$ the slope (46) is positive and an increase in the secondary load σ_y^{∞} increases the critical load σ_{cx}^{∞} necessary to originate a debond, see Figure 14. This is the case of the two bimaterials defined in Table 1, i.e. glass/epoxy and carbon/epoxy. However, an opposite effect is predicted for $k/m > 1$, see Figure 14. In fact, this dependence matches up with the effect of the secondary load σ_y^{∞} predicted by

Goodier's solution for the interface point $\theta = 0°$, see (1), which shows that a compression or tension is expected at $\theta = 0°$ when a secondary load $\sigma_y^\infty > 0$ is applied for $k/m < 1$ or $k/m > 1$, respectively.

The present results show that the influence of the secondary load σ_y^∞ on the critical load σ_{cx}^∞ is at most moderate in usual composites. Taking into account that in the case $\gamma \to 0^+$, analysed in Figure 14, the values of σ_{cx}^∞ are the most sensitive to the values of σ_y^∞, in general for $k/m < 1$ the influence of σ_y^∞ on the value of σ_{cx}^∞ exists but it is small or at most moderate. For bimaterials as glass/epoxy and carbon/epoxy with $\frac{k}{m} < 1$, these results agree with the hypothesis introduced by París et al. (2003). According to this hypothesis a secondary compression σ_y^∞ makes easier the debond onset for these bimaterials and reduces the critical load σ_{cx}^∞ as shown in Figure 14(b). However, for bimaterials with $\frac{k}{m} > 1$ the effect is opposite, a secondary compression $\sigma_y^\infty < 0$ increases the critical load σ_{cx}^∞.

4.4. Post-onset evolution

After the onset of a new crack, an unstable growth of the crack is possible depending on the relation between $G(\theta_d)$ and $G_c(\theta_d)$ for $\theta_d \geq \theta_c$ and according to the criterion of the classical (infinitesimal) interface fracture mechanics (see, e.g. París et al. (2007); Mantič et al. (2006)). Thus, the condition for the further crack growth will be

$$G(\theta_d, \eta) \geq G_c(\psi(\theta_d, \eta)), \qquad \theta_d \geq \theta_c. \tag{47}$$

The crack will stop growing at an arrest angle $\theta_a \geq \theta_c$ verifying $G(\theta_a, \eta) = G_c(\psi((\theta_a, \eta))$ if for angles $\theta_d \gtrsim \theta_a$ criterion (47) is not fulfilled. The stability of the post-onset growth of the crack is different for two scenarios A and B separated by γ_{th} two post-onset scenarios being possible:

- For $\gamma < \gamma_{\text{th}}$, $G(\theta_c, \eta) > G_c(\psi(\theta_c, \eta))$ and the crack is expected to continue growing in an unstable manner up to an arrest angle $\theta_a > \theta_{\text{min}}^E$, which can be shown similarly as in Mantič (2009).
- For $\gamma \geq \gamma_{\text{th}}$, $\theta_c = \theta_{\text{min}}^E$, $G(\theta_c, \eta) = G_c(\psi(\theta_c, \eta))$ and $\mathrm{d}G/\mathrm{d}\theta_d|_{\theta_d = \theta_{\text{min}}^E} \leq \mathrm{d}G_c/\mathrm{d}\theta_d|_{\theta_d = \theta_{\text{min}}^E}$, see (31) and related discussion in Subsection 4.2. Therefore, assuming strict inequality in (31) (which, in fact, has been verified in all present calculations), no unstable crack growth is usually expected after the crack onset and $\theta_a = \theta_{\text{min}}^E$.

Figures 11(a) and 15 were computed by implementing the above ideas. The values of G and G_c and their derivatives are compared for $\theta_d \geq \theta_c$ in order to find the arrest semiangle θ_a. According to these figures, a long unstable crack growth after the crack onset is predicted for small values of γ (brittle configurations), whereas short (or zero) unstable crack growth is predicted for large vales of γ (tough configurations).

4.5. Applicability of the open model of interface cracks

The applicability of the theoretical model developed is limited by its assumptions, perhaps the most restrictive being the usage of the open model of interface cracks. Toya's (1974) solution assumes negligible overlapping of traction-free crack faces. The angle of the overlapping zone at the crack tip can be estimated by the formula deduced by Hills and Barber (1993) and generalized by Graciani et al. (2007), which rewritten for the present case is defined as the largest value of

$$\theta_I(\theta_d, \eta) = \theta_l \cdot \exp\left[\left((2n - 1/2)\,\pi - \psi(\theta_d, \eta, \theta_l)\mathrm{sign}\varepsilon \;+\; \arctan(2\,|\varepsilon|)\right) / \,|\varepsilon|\right], \tag{48}$$

lower than the semidebond angle θ_d, with n being an integer.

Figure 16 shows the evolutions of $\hat{G}$ for glass/epoxy and different values of the load biaxiality parameter η. Additionally, for $\gamma = 1.5$, corresponding to relatively tough configurations, the values of θ_c, θ_{min}^E and θ_a computed by the present model are indicated. Finally, angles $\theta_{I,1\%}$ for which the overlapping zone represent 1% of the crack length, i.e. $\theta_I/2\theta_d = 0.01$, providing a reasonable limit of validity of the open model, are also presented in Figure 16. This figure shows that all the values of θ_c are lower than the reference limit $\theta_{I,1\%}$, therefore the open model is acceptable for the evaluation of θ_c and the critical load σ_{cx}^∞. However, it might not be fully acceptable when computing θ_a for large negative values of η. Note that, the above discussed limit on the semiangle θ_d is mainly due to somewhat inaccurate evaluation of

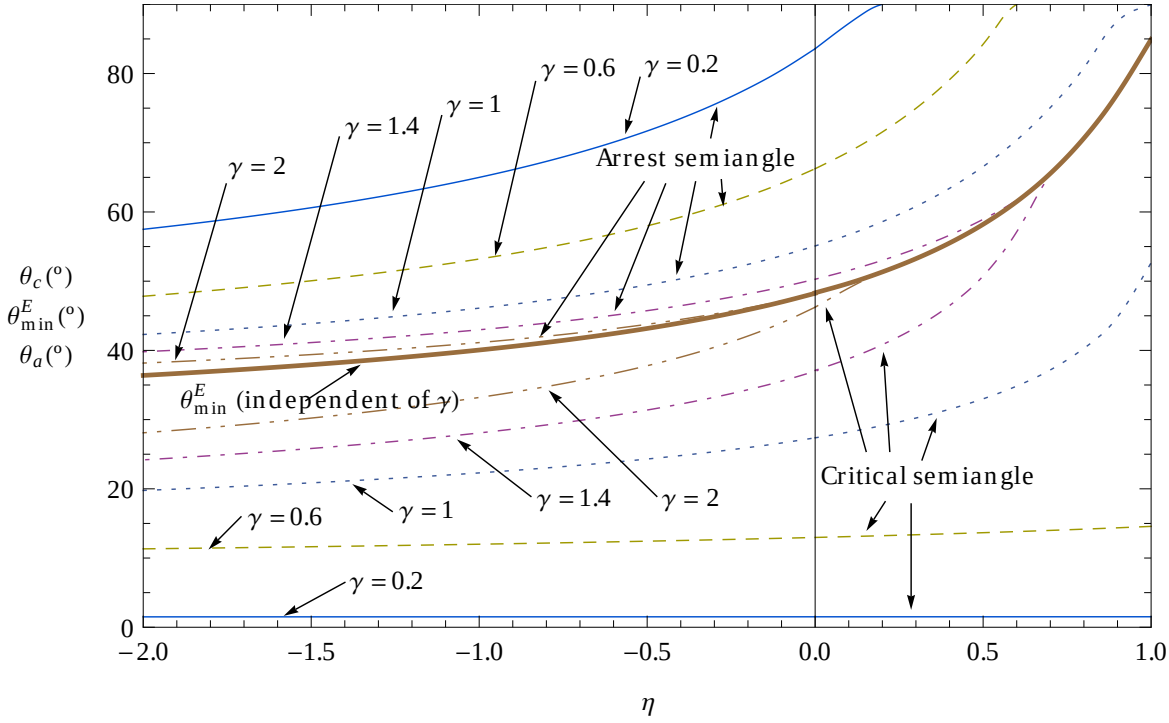

Figure 15: Semiangles θ_c, $\theta^E_{\min}$ and θ_a as functions of the biaxiality parameter η for different values of γ, taking $\theta_l = 0.1°$, $\lambda = 0.3$ and glass/epoxy.

$\hat{G}$ because of a large overlapping zone at the crack tip, see also Figure 6 and the related discussion. A correct procedure for the evaluation of $\hat{G}$ is such cases would require employing the contact model of interface cracks as in París et al. (2007) and Correa (2008).

5. Size effect of the inclusion radius a on the crack onset and its variations with the biaxiality

A size effect in the present debond onset problem can be understood as a dependence of the critical remote load (σ^∞_{cx},σ^∞_{cy}) and critical semiangle θ_c on the only geometrical parameter in the present problem, the inclusion radius a. As will be seen, this size effect is directly related to the brittle-to-tough transition governed by the brittleness number γ, see Figure 11.

Let a bimaterial characteristic length a_0 be defined in terms of the interface properties σ_c and G_{1c} and the harmonic mean of effective Young moduli E^*,

$$a_0 = \frac{G_{1c}E^*}{\sigma_c^2}. \tag{49}$$

Then, the normalized radius $\frac{a}{a_0}$ and γ are related by

$$\gamma = \sqrt{\frac{a_0}{a}}. \tag{50}$$

Analogously to the threshold value γ_{th} (41), a threshold value of a is defined as

$$a_{\text{th}} = \frac{a_0}{\gamma_{\text{th}}^2}. \tag{51}$$

In fact, all the analysis presented above taking as reference γ can be expressed as a dependence on a in an analogous manner. For sufficiently large values of a, which correspond to small values of γ, the

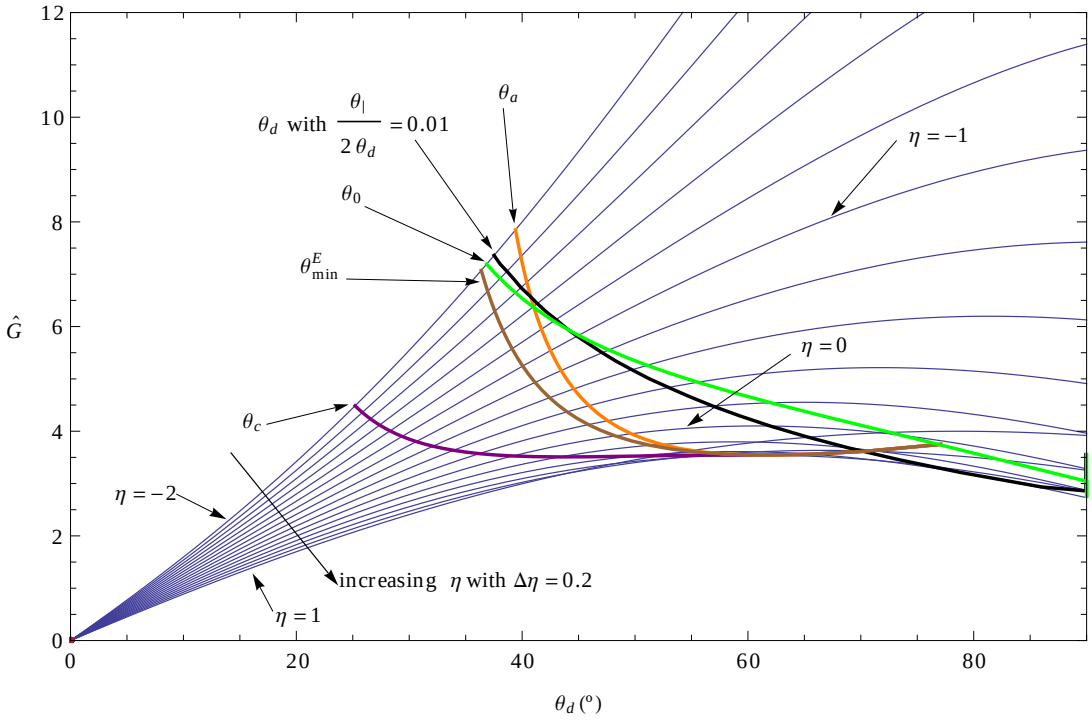

Figure 16: Plots of evolution of values of dimensionless ERR limited by the semiangles which estimate the validity of the model and representation of important values of semiangles of the results, taking $\lambda = 0.3$, $\theta_l = 0.1°$, $\gamma = 1.5$ for glass/epoxy.

critical semiangle θ_c and the critical remote load σ^∞_{cx} can be approximated by the following expressions, see Section 4,

$$\theta_c \cong \frac{2\cosh^2(\pi\varepsilon)}{\pi(1+4\varepsilon^2)}\frac{a_0}{a} \quad \text{and} \quad \frac{\sigma^\infty_{cx}}{\sigma_c} \cong \frac{1}{k+(k-m)\eta}, \tag{52}$$

whereas for $a \leq a_{\text{th}}$,

$$\theta_c = \theta^E_{\min} \quad \text{and} \quad \frac{\sigma^\infty_{cx}}{\sigma_c} = \sqrt{g(\theta^E_{\min},\eta)}\sqrt{\frac{a_0}{a}}. \tag{53}$$

As follows from (52) and (53), the critical crack-semilength $a\theta_c$ is constant and independent of a and η for large a, whereas for small a it is linearly proportional a.

The above described asymptotic behaviour of θ_c and σ^∞_{cx} can be easily identified in Figure 17 where the variations of θ_c, θ_a and σ^∞_{cx} as functions of a are plotted. In particular, in Figure 17(a) and (b) it is seen that $\theta_c = \theta_a = \theta^E_{\min}$ and $\sigma^\infty_{cx} \approx 1/\sqrt{a}$, respectively, for $a \leq a_{\text{th}}$. Thus, σ^∞_{cx} increases drastically for small inclusions while for large inclusions it tends to a constant value given by the stress criterion applied at $\theta = 0°$. As can be observed in Figure 17(b), the size effect on σ^∞_{cx} is similar for different values of η, being quite independent of the combination of remote transverse loads.

6. Experimental procedure for the measurement of the brittleness number γ, interfacial tensile strength σ_c and fracture toughness G_{1c}

Fracture properties of the fibre-matrix interfaces are very important for the macroscopic behaviour of fibre reinforced composites. However the experimental measurement of these is very difficult to be carried out. An indirect experimental procedure is proposed here for obtaining first the value of γ, and subsequently the values of σ_c and G_{1c}, for a bimaterial. Elastic properties of the bimaterial (E^*, α, β) are

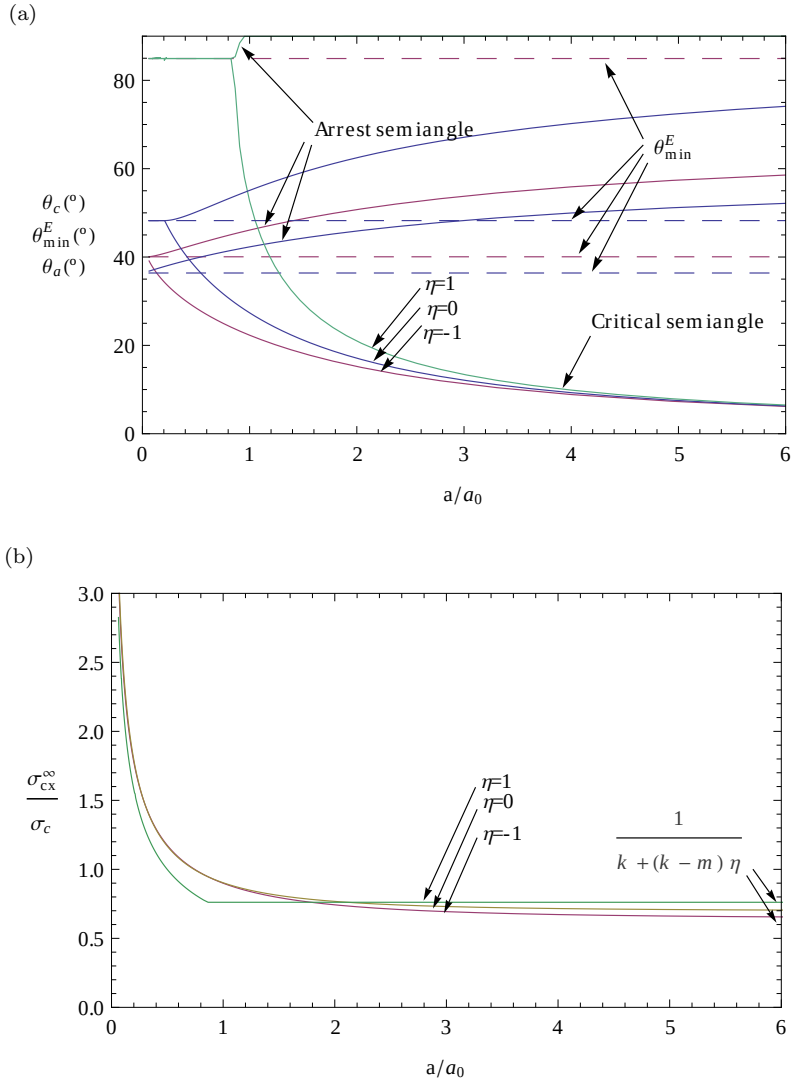

Figure 17: (a) Critical semiangle θ_c and (b) Critical remote tension in σ^∞_{cx} as a function of the inclusion radius a, taking $\lambda = 0.3$, $\theta_l = 0.1°$ and glass/epoxy.

assumed to be known, as they can be measured by carrying out standard material tests for each material separately.

To determine the interface properties, the sole measure of the critical stress for the case of remote uniaxial tension ($\eta = 0$) is not sufficient. The reason is that the critical stress depends not only on γ but also on σ_c, see the normalization used in (38). Nevertheless, if the critical stress is also measured for a biaxial load ($\eta \neq 0$), then, the ratio of these critical stresses depends only on the value of γ due to the influence of γ value on the solution θ_c of (37). This is the key idea behind the experimental procedure proposed. This procedure employs plots of the ratio of critical stresses $\frac{\sigma^\infty_{cx}(\eta\neq 0)}{\sigma^\infty_{cx}(\eta=0)}$ as a function of γ or η. As an example, Figure 18 shows values of $\frac{\sigma^\infty_{cx}(\eta\neq 0)}{\sigma^\infty_{cx}(\eta=0)}$ for glass/epoxy, taking $\theta_l = 0.1°$ and $\lambda = 0.3$.

The steps of the experimental procedure are briefly explained in the following:

1. Determine the critical stress σ^∞_{cx} in the uniaxial tension test ($\eta = 0$). This is a relatively easy test, thus a good accuracy is expected.
2. Determine another critical stress σ^∞_{cx} in a biaxial test for $\eta \neq 0$. Combining the plots in Figure 18(a) and a rough *a priori* estimation of the γ value, choose the most suitable value of η to test by looking

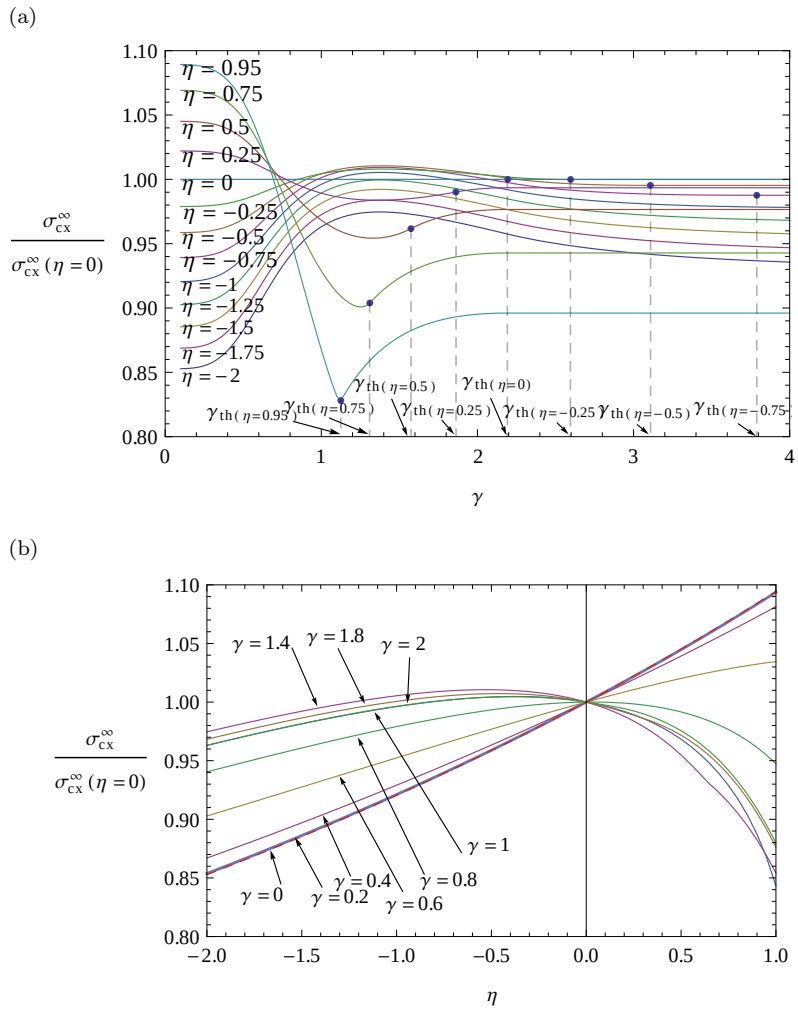

Figure 18: Graphs for determination of γ by applying the experimental procedure proposed. Predictions for $\frac{\sigma_{cx}^{\infty}(\eta)}{\sigma_{cx}^{\infty}(\eta=0)}$ as a function of (a) γ and (b) η for glass/epoxy, $\theta_l = 0.1°$ and $\lambda = 0.3$.

for an invertible segment of the pertinent function plotted in Figure 18(a) and for its maximum slope. Capabilities of the testing machine may represent an additional constraint.

3. Evaluate the ratio of the measured critical stress $\frac{\sigma_{cx}^{\infty}(\eta\neq 0)}{\sigma_{cx}^{\infty}(\eta=0)}$. Then, estimate a value of $\tilde{\gamma}$ from the measured ratio of the critical stresses for the chosen value of η from Figure 18(a).
4. Estimate a value of the critical semiangle θ_c by solving the following nonlinear equation, employing $\tilde{\gamma}$, see (37):

$$\tilde{\gamma}\sqrt{g(\tilde{\theta}_c,\eta)} = s(\tilde{\theta}_c,\eta) \tag{54}$$

5. Estimate the interfacial tensile strength σ_c from (38),

$$\tilde{\sigma}_c = \frac{\tilde{\sigma}_{cx}^{\infty}(\eta)}{\tilde{\gamma}\sqrt{g(\tilde{\theta}_c,\eta)}}, \tag{55}$$

where $\tilde{\sigma}_{cx}^{\infty}$ is one of the two values measured, either for $\eta = 0$ or $\eta \neq 0$.

6. Estimate the interfacial fracture toughness G_{1c} from (36)

$$\tilde{G}_{1c} = \frac{(\tilde{\sigma}_c \tilde{\gamma})^2 \, a}{E^*}. \tag{56}$$

A few comments follow with reference to a possible stumbling block tackled in the 2nd step of the above procedure.

As can be observed from Figure 18(a), the ratio $\frac{\sigma_{cx}^{\infty}(\eta \neq 0)}{\sigma_{cx}^{\infty}(\eta = 0)}$ for a given η is not an injective (one-to-one) function of γ for the whole range of γ considered. Nevertheless, this ratio may become an injective function of γ when restricted to a suitable interval of γ, e.g. to small values of γ roughly in the range $0 < \gamma \lesssim 1$. In general, an a priori estimate of γ will be very useful in choosing a suitable $\eta \neq 0$ for the biaxial test and a pertinent interval of γ where the above ratio is an injective function.

Recall that for $\gamma > \gamma_{\text{th}}$ the critical semiangle is constant ($\theta_c = \theta_{\text{min}}^E$) and the energy criterion determines the critical remote tension, which is directly proportional to γ, see (40). Then, for a given value of η, the value of $\sqrt{g(\theta_{\text{min}}^E(\eta), \eta)}$ is fixed. Thus, the ratio shown in Figure 18(a) for $\gamma \geq \gamma_{\text{th}}(\eta)$ and $\gamma \geq \gamma_{\text{th}}(\eta = 0)$ is

$$\frac{\sigma_{cx}^{\infty}(\eta)}{\sigma_{cx}^{\infty}(\eta = 0)} = \frac{\sqrt{g(\theta_{\text{min}}(\eta), \eta)}}{\sqrt{g(\theta_{\text{min}}(\eta = 0), \eta = 0)}}. \tag{57}$$

Hence, this ratio is a constant independent of γ, as can be observed in Figure 18(a). Obviously for these rather large values of γ, the proposed experimental procedure (including the biaxial test for only one value of η) is not directly applicable.

Nevertheless, repeating the biaxial tests for several adequately chosen values of η and applying least square fitting to functions plotted in Figure 18(b) could provide a good estimation of γ, and subsequently of σ_c by (55) and G_{1c} by (56) as well.

7. Concluding Remarks

1. The problem of the onset of a debond of a finite length at the initially undamaged interface of a circular cylindrical inclusion embedded in an infinite matrix subjected to a remote biaxial transverse load has been studied. A theoretical model has been developed assuming linear elastic plane strain states before and after the debond onset and sufficiently dilute packing. The critical biaxial load leading to the onset of a debond symmetrically situated with respect to the dominating remote tension is predicted together with the debond size. The present model is based on the Finite Fracture Mechanics approach introduced by Leguillon (2002) combining a pointwise normal tension criterion with an incremental energy criterion.
   It is expected that the present work will contribute to the knowledge of the governing parameters and to overall understanding of the failure mechanism in the fiber composites under tension dominated transverse loads. A special attention has been given to the influence of a secondary compression/tension on the value of the critical (primary) tension. Although the present work is focused on a stiff inclusion embedded in a compliant matrix (glass/epoxy composite has been used as a representative example), most results are generally valid for any combination of elastic bimaterial parameters.
   For the sake of simplicity a remote biaxial stress state $(\sigma_x^{\infty}, \sigma_x^{\infty})$ with $\sigma_{xy}^{\infty} = 0$ is assumed. Nevertheless, the present model and results may be easily adapted to a general remote in-plane stress state with $\sigma_{xy}^{\infty} \neq 0$ by working in its principal coordinate system and assuming that at least one principal stress is tension.
2. The predictions of the present model are governed by the dimensionless brittleness number γ introduced for interface cracks in Mantič (2009). A consequence of this fact is that a size effect on the critical remote load and on the size of the debond at onset is predicted by the present model.
   It may be useful to realize that an alternative brittleness number given in terms of the critical Stress Intensity Factor (SIF) in fracture Mode I K_{1c}, instead of the critical ERR G_{1c}, can be proposed. Taking into account the relation between the complex Stress Intensity Factor K and

Energy Release Rate G in interfacial fracture mechanics (see Malyshev and Salganik (1965)) $G = |K|^2/(E^* \cdot \cosh^2(\pi\varepsilon))$, this alternative brittleness number is expressed as

$$\gamma_K = \gamma \cdot \cosh(\pi\varepsilon) = \frac{K_{1c}}{\sigma_c}\frac{1}{\sqrt{a}}. \tag{58}$$

Recall that the expression of γ_K in terms of K_{1c} reminds the classical definition of the brittleness number s in homogeneous materials by Carpinteri (1981). Note that, $\varepsilon = 0$ for a crack in a homogeneous material, thus $\gamma_K = \gamma$ in this case.

3. The way how the remote secondary load σ_y^∞ influence the critical value of remote tension σ_{cx}^∞ depends on the value of the ratio $k/m = \frac{1}{2}\frac{2+\alpha-\beta}{1+\alpha-2\beta}$, defined in terms of the Dundurs elastic bimaterial parameters α and β. In particular, for $\gamma \ll 1$, a remote secondary compression σ_y^∞ decreases or increases σ_{cx}^∞ if $k/m < 1$ or $k/m > 1$, respectively. This result, for $k/m < 1$, is coherent with the hypothesis proposed and experimentally verified by París et al. (2003) for a particular carbon/epoxy composite.
   For moderate or larger values of γ, $\gamma \gtrsim 1$, this model predicts an almost negligible influence of the secondary compression σ_y^∞ on the critical tension σ_{cx}^∞ for the glass/epoxy bimaterial studied, having a somewhat flat maximum for $\eta \lesssim 0$ (see Figure 12). This observation is related to the fact that the critical semidebond angles θ_c predicted for these values of γ are sufficiently large to make the influence of the secondary compression σ_y^∞ more complex. However, the latter conclusions should be accepted with a caution in view of the range of model applicability, which appears to be very suitable for brittle configurations but to a lesser extent for tough ones.
4. In addition to the inclusion-matrix debond onset mechanism studied in the present work, other failure mechanisms can occur in the inclusion-matrix system under remote transverse loads. This is, for example, the case of the dominating compressive load studied by the coupled stress and energy criterion in Quesada et al. (2009), where parallel cracks in the inclusion and the matrix are predicted. Another example of inclusion-matrix debond configurations not allowed by the present assumption of the debond symmetrically situated with respect to the principal directions of the remote load were studied in Correa et al. (2008). Experimental tests of specimens subjected to remote transverse compressions show debonds originating at interface positions with large shear stresses. Thus, in order to complete the picture of failure envelopes shown in Figure 12, such configurations should be studied in a similar way as done in the present work. In order to take into account the influence of interface shear stresses, the stress criterion should be revised. The Mohr-Coulomb criterion (used in brittle materials and soil mechanics, see Carpinteri (1986) for a review) appears to be a suitable candidate as it shows a good agreement with the experiments carried out by Toda et al. (2001) and Ogihara and Koyanagi (2010) about failures at interfaces.

Acknowledgements

The authors thank to Prof. F. París for his motivation and continuous support of the present work. The authors also thank to Dr. E. Correa for her Mathematica code of Toya's solution used for checking proposes. This work was supported by the Junta de Andalucía and the Spanish Ministry of Science and Innovation, through the Projects TEP4051 and MAT2009-14022, respectively. I.G. García also acknowledges the support by the Spanish Ministry of Education through the FPU Grant 2009/3968.

Appendix A. Domain of existence on the angle θ_0 where normal traction vanishes

A threshold parameter η_0 can be defined as

$$\eta_0(\alpha,\beta) = \left(\frac{k}{m}\right)^{-1} - 1. \tag{A.1}$$

It will be useful to know the range of this parameter given in terms of the values of k/m,

$$\eta_0 \in \underbrace{(-1,0]}_{\frac{k}{m}\geq 1} \cup \underbrace{(0,1/3]}_{3/4\leq \frac{k}{m}<1} . \tag{A.2}$$

Then, the expression on the right-hand side of (8) makes sense for $\eta < 1$ only if

$$\begin{cases} \eta \leq \eta_0 & \text{if } \frac{3}{4} \leq \frac{k}{m} \leq 1, \\ \frac{1}{\eta_0} \leq \eta \leq \eta_0 & \text{if } \frac{k}{m} > 1. \end{cases} \tag{A.3}$$

As can be seen in Figure A.1, only tensions (compressions) take place along the whole interface for $\eta > \eta_0$ (for $\eta < 1/\eta_0$ and $\frac{k}{m} > 1$).

It will be convenient to extend the definition of θ_0 defining $\tilde{\theta}_0$ as follows

$$\tilde{\theta}_0\,(\eta;\alpha,\beta) = \begin{cases} \theta_0, & \exists\theta_0, \text{ see } (A.3), \\ 90°, & \eta_0 \leq \eta \leq 1, \\ \nexists, & \eta < 1/\eta_0 \text{ and } k/m > 1. \end{cases} \tag{A.4}$$

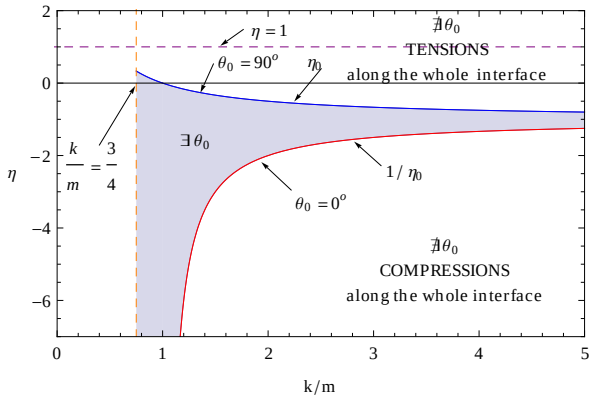

Figure A.1: Domain of definition of an angle $\theta_0 \in [0°, 90°]$ along the interface where the normal tractions vanish as a function of the elastic bimaterial parameter k/m and the biaxiality parameter η for $\sigma_x^\infty > 0$.

Appendix B. Functions χ and p of the expression of Toya for stresses along the interface with a partial debond

$$\chi(\theta,\theta_d,\beta) = (e^{i\theta} - e^{i\theta_d})^{-(1/2)-i\varepsilon}(e^{i\theta} - e^{-i\theta_d})^{-1/2+i\varepsilon}, \tag{B.1}$$

$$p(\theta,\theta_d,\eta,\beta) = q(\theta_d,\eta,\beta)(e^{i\theta} - (\cos\theta_d - 2\varepsilon\sin\theta_d)) - \frac{1+\alpha}{1-\alpha}(1-\eta)e^{2\varepsilon(\pi-\theta_d)-i\theta}(\cos\theta_d + 2\varepsilon\sin\theta_d - e^{-i\theta}), \tag{B.2}$$

with

$$q(\theta_d,\eta,\beta) = \left[(1+\eta)(1-(\cos\theta_d - 2\varepsilon\sin\theta_d)e^{2\varepsilon(\theta_d-\pi)}) + \frac{1}{2}(1+\alpha)(1+4\varepsilon^2)(1-\eta)\sin^2\theta_d\right] / \\ / \left[3+\alpha-(1-\alpha)(\cos\theta_d - 2\varepsilon\sin\theta_d)e^{2\varepsilon(\theta_d-\pi)}\right] - \frac{1+\eta}{1-\alpha}. \tag{B.3}$$

where $i = \sqrt{-1}$ is the imaginary unit, and

$$\varepsilon = (1/2\pi)\ln(1-\beta)/(1+\beta) \tag{B.4}$$

is the so-called oscillation index (see Table 1).

Appendix C. Expression of the dimensionless ERR $\hat{G}$

$$\hat{G}(\theta_d,\eta,\alpha,\beta) = \frac{\pi}{4}e^{-2\varepsilon(\pi-\theta_d)}(\alpha-1)^2\left(1+4\varepsilon^2\right)||c(\theta_d,\eta,\alpha,\beta)+d(\theta_d,\eta,\alpha,\beta)||^2\cdot\sin\theta_d, \tag{C.1a}$$

with

$$c(\theta_d,\eta,\alpha,\beta) = \left[-\frac{1}{2}(1+\alpha)\left(1+4\varepsilon^2\right)(\eta-1)\sin(\theta_d)^2 + (1+\eta)\left(1-e^{2\varepsilon(\pi-\theta_d)}(2\varepsilon\sin(\theta_d)-\cos(\theta_d))\right)\right] / \left[3+\alpha+e^{-2\varepsilon(\pi-\theta_d)}(\alpha-1)(\cos(\theta_d)-2\varepsilon\sin(\theta_d))\right] \tag{C.1b}$$

and

$$d(\theta_d,\eta,\alpha,\beta) = \frac{1-e^{2\varepsilon(\pi-\theta_d)-i\theta_d}(1+\alpha)(\eta-1)+\eta}{\alpha-1}. \tag{C.1c}$$

Appendix D. Asymptotic analysis for a vanishing critical semiangle

For a vanishing crack semiangle, the derivatives of $\hat{G}$ and G with respect to the crack semiangle and semilength respectively are,

$$\left.\frac{\mathrm{d}\hat{G}}{\mathrm{d}\theta_d}\right|_{\theta_d=0} = (k+(k-m)\eta)^2\,\frac{\pi\left(1+4\varepsilon^2\right)}{\cosh^2(\pi\varepsilon)}, \tag{D.1}$$

$$\left.\frac{\mathrm{d}G}{\mathrm{d}(a\theta_d)}\right|_{\theta_d=0} = \left[(k+(k-m)\eta)\,\sigma_x^\infty\right]^2\,\frac{\pi\left(1+4\varepsilon^2\right)}{E^*\cosh^2(\pi\varepsilon)}. \tag{D.2}$$

This expressions agree with the analogous derivative of ERR seen in Rice (1988) for a crack at a straight interface. It is instructive to notice that the factor $(k+(k-m)\eta)$ agrees with the concentration factor of normal tractions $\sigma(\theta)$ obtained from Goodier's solution at $\theta = 0°$, see (5a) and (7)

On the other hand, the function g in (28) can be approximated for small values of $\Delta\theta$. As $\psi(\theta_d)$ is small for small θ_d, thus $\tan^2(1-\lambda)\psi$ is negligible with respect to the unity and $G_c(\psi) \gtrapprox G_{1c}$. Then, using (D.1), for small $\Delta\theta$,

$$g(\Delta\theta,\eta;\alpha,\beta;\lambda,\theta_l) \gtrsim \tilde{g}(\Delta\theta;\eta;\alpha,\beta) = \frac{2}{\hat{G}'(0°;\eta;\alpha,\beta)\cdot\Delta\theta} = \frac{\cosh^2(\pi\varepsilon)}{\pi\left(1+4\varepsilon^2\right)(k+(k-m)\eta)^2}\frac{2}{\Delta\theta}, \tag{D.3}$$

where the asymptotic approximation function $\tilde{g}$ is smaller than the exact function g, see Figure 9.

Then, combining the approximation of g in (D.3) and equation (37), θ_c can be approximated by

$$\theta_c \cong \frac{2(k+(k-m)\eta)^2}{\hat{G}'(0)}\gamma^2 = \frac{2\cosh^2(\pi\varepsilon)}{\pi(1+4\varepsilon^2)}\gamma^2 \quad \text{for} \quad \gamma\to 0^+. \tag{D.4}$$

Note that, the asymptotic solution is independent of the load biaxiality parameter η. Therefore, for small values of γ, the effect of the remote secondary load σ_y^∞ on the semiangle of the crack originated is negligible.

Appendix E. Partitioning of $\hat{G}$ into two components corresponding in some sense to modes I and II

ERR based measure of fracture mode mixity, angle ψ_G, is defined in terms of G_I and G_{II} as follows

$$\tan^2 \psi_G = \frac{G_{II}}{G_I} = \frac{\hat{G}_{II}}{\hat{G}_I}. \tag{E.1}$$

According to Mantič and París (2004), the ERR and the SIF based measures of mode mixity, phase angles ψ and ψ_G, respectively, can be related by the following expression:

$$\cos(2\psi_G) = F(\varepsilon)\cos\left[2(\psi + \psi_0(\delta\theta/\theta_l, \varepsilon))\right], \tag{E.2}$$

where

$$F(\varepsilon) = \sqrt{\frac{\sinh(2\pi\varepsilon)}{2\pi\varepsilon(1+4\varepsilon^2)}}, \tag{E.3}$$

and

$$2\psi_0(\delta\theta/\theta_l, \varepsilon) = 2\varepsilon\ln(\delta\theta/2\theta_l) + \varphi(\varepsilon) - \arctan(2\varepsilon) \tag{E.4}$$

with

$$\varphi(\varepsilon) = \arg\left[\frac{\Gamma(1/2+i\varepsilon)}{\Gamma(1+i\varepsilon)}\right], \tag{E.5}$$

$\Gamma(\cdot)$ being the gamma function.

Combining (E.1), (E.2) and some trigonometric identities, the value of $\hat{G}_I(\theta_d, \delta\theta)$ and $\hat{G}_{II}(\theta_d, \delta\theta)$ can be expressed in terms of $\psi(\theta_l)$ as,

$$\hat{G}_{I,II}(\theta_d, \delta\theta) = \frac{1}{2}\hat{G}(\theta_d)(1 \pm F(\varepsilon)\cos(2(\psi(\theta_d, \theta_l) + \psi_0(\delta\theta/\theta_l, \varepsilon))). \tag{E.6}$$

Appendix F. Expressions for computational proposes

Combining the upper limit given by θ_0 in (22), those for the existence of θ_0 in (A.3) with the stress condition in (19), and the condition of minimal load (20), a maximum semiangle of a debond for a given load according to the stress criterion is defined as

$$\theta_c^\sigma\left(\frac{\sigma_x^\infty}{\sigma_c}, \eta; \alpha, \beta\right) = \begin{cases} \nexists, & (\eta \le 1/\eta_0 \text{ and } k/m > 1) \text{ or } \frac{\sigma_x^\infty}{\sigma_c} < \frac{1}{k+(k-m)\eta}, \\ 180^\circ, & \eta > \eta_0 \text{ and } \frac{\sigma_x^\infty}{\sigma_c} \ge \frac{1}{k(1+\eta)-m}, \\ \arcsin\sqrt{\frac{k+(k-m)\eta-\frac{\sigma_c}{\sigma_x^\infty}}{(1-\eta)m}}, & \text{in other cases.} \end{cases} \tag{F.1}$$

In the same sense, the dimensionless function $s(\theta)$ can be generalized for $\theta \in [0^\circ, 180^\circ]$ as

$$s(\theta, \eta; \alpha, \beta) = \begin{cases} \frac{1}{k+(k-m)\eta-(1-\eta)m\sin^2\theta}, & \exists\tilde{\theta}_0 \text{ and } \theta < \tilde{\theta}_0, \\ +\infty, & \exists\theta_0 \text{ and } \theta \ge \theta_0, \\ \frac{1}{k(1+\eta)-m}, & \eta > \eta_0 \text{ and } \theta \ge 90^\circ, \\ +\infty, & \eta \le 1/\eta_0 \text{ and } k/m > 1. \end{cases} \tag{F.2}$$

Then, the present stress criterion can be written in a general form as follows: an interface debond onset

of an angle $2\Delta\theta$ (symmetrical with respect to the x-axis) is possible if

$$\frac{\sigma_x^\infty}{\sigma_c} \geq s(\Delta\theta, \eta), \tag{F.3}$$

θ_c^σ representing the upper limit for the semiangles $\Delta\theta$ verifying (F.3) for a given remote load.

Appendix G. Proof of inequality $\frac{\mathrm{d}G}{\mathrm{d}\theta_d} \leq \frac{\mathrm{d}G_c}{\mathrm{d}\theta_d}$ for $\theta_d = \theta_c^E = \theta_{\min}^E$

For the sake of simplicity, the following notation will be used $G(\theta_d) = G(\theta_d; \sigma_x^\infty, \eta; a; E^*, \alpha, \beta)$ and $G_c(\theta_d) = G_c(\psi(\theta_d, \eta), G_{1c}, \lambda)$. Recall that θ_c^E is defined as the minimum positive angle for which the equality in (26), or equivalently in (27), hold. Then, if $\theta_c^E = \theta_{\min}^E$,

$$\int_0^{\Delta\theta} G(\theta_d)\mathrm{d}\theta_d < \int_0^{\Delta\theta} G_c(\theta_d)\mathrm{d}\theta_d \quad \text{for} \quad 0 < \Delta\theta < \theta_{\min}^E, \tag{G.1}$$

and

$$\int_0^{\theta_{\min}^E} G(\theta_d)\mathrm{d}\theta_d = \int_0^{\theta_{\min}^E} G_c(\theta_d)\mathrm{d}\theta_d. \tag{G.2}$$

By substracting (G.1) from (G.2),

$$\int_{\Delta\theta}^{\theta_{\min}^E} G(\theta_d)\mathrm{d}\theta_d > \int_{\Delta\theta}^{\theta_{\min}^E} G_c(\theta_d)\mathrm{d}\theta_d \quad \text{for} \quad 0 < \Delta\theta < \theta_{\min}^E. \tag{G.3}$$

Let $G(\theta_d)$ and $G_c(\theta_d)$ be approximated by Taylor polynomials centered at $\theta_d = \theta_{\min}^E$,

$$G(\theta_d) \approx G(\theta_{\min}^E) + \left.\frac{\mathrm{d}G}{\mathrm{d}\theta_d}\right|_{\theta_d=\theta_{\min}^E} (\theta_d - \theta_{\min}^E) + O\left((\theta_d - \theta_{\min}^E)^2\right), \tag{G.4a}$$

$$G_c(\theta_d) \approx G_c(\theta_{\min}^E) + \left.\frac{\mathrm{d}G_c}{\mathrm{d}\theta_d}\right|_{\theta_d=\theta_{\min}^E} (\theta_d - \theta_{\min}^E) + O\left((\theta_d - \theta_{\min}^E)^2\right). \tag{G.4b}$$

Then, introducing (G.4) in (G.3) and integrating the Taylor polynomials, the following inequality is obtained, denoting $h = \theta_{\min}^E - \Delta\theta$:

$$G(\theta_{\min}^E)h - \left.\frac{\mathrm{d}G}{\mathrm{d}\theta_d}\right|_{\theta_d=\theta_{\min}^E} \frac{h^2}{2} + O\left(h^3\right) > G_c(\theta_{\min}^E)h - \left.\frac{\mathrm{d}G_c}{\mathrm{d}\theta_d}\right|_{\theta_d=\theta_{\min}^E} \frac{h^2}{2} + O\left(h^3\right) \quad \text{for} \quad 0 < h < \theta_{\min}^E. \tag{G.5}$$

Hence, taking into account that $G(\theta_{\min}^E) = G_c(\theta_{\min}^E)$ from (30) and considering (G.5) for vanishing $h > 0$,

$$\left.\frac{\mathrm{d}G}{\mathrm{d}\theta_d}\right|_{\theta_d=\theta_{\min}^E} \leq \left.\frac{\mathrm{d}G_c}{\mathrm{d}\theta_d}\right|_{\theta_d=\theta_{\min}^E}, \tag{G.6}$$

otherwise (G.5) could not hold for a sufficiently small $h > 0$.

References

Carpinteri, A. (1981). Size effect in fracture toughness testing: a dimensional analysis approach. In G. Sih and M. Mirabile (Eds.), *Analytical and Experimental Fracture Mechanics*, pp. 785–797. International Conference on Analytical and Experimental Fracture Mechanics, Roma, Italy, 1980.

Carpinteri, A. (1986). *Mechanical Damage and Crack Growth in Concrete*. Martinus Nijhoff Publishers, Dordrecht.

Carpinteri, A., M. Paggi, and G. Zavarise (2005). Snap-back instability in micro-structured composites and its connection with superplasticity. *Strength, Fracture and Complexity 3*, 61 – 72.

Cornetti, P., N. Pugno, A. Carpinteri, and D. Taylor (2006). Finite fracture mechanics: A coupled stress and energy failure criterion. *Engineering Fracture Mechanics 73*, 2021–2033.

Correa, E. (2008). *Micromechanical analysis of the matrix failure in fibre reinforced composites (In Spanish)*. Ph. D. thesis, School of Engineering, University of Seville.

Correa, E., V. Mantič, and F. París (2008). Numerical characterisation of the fibre-matrix interface crack growth in composites under transverse compression. *Engineering Fracture Mechanics 75*, 4085–4103.

Dundurs, J. (1967). Effect of elastic constants on stress in a composite under plane deformations. *Journal of Composite Materials 1*, 310–322.

Dundurs, J. (1969). Discussion of a paper by D.B. Bogy. *Journal of Applied Mechanics 36*, 650–652.

García, I. G., V. Mantič, and E. Graciani (2012). Debonding at the fibre-matrix interface under remote tranverse tension. one or two symmetric debonds? *(to be submitted)*.

Goodier, J. (1933). Concentration of stress around spherical and cylindrical inclusions and flaws. *Journal of Applied Mechanics 55*, 39–44.

Graciani, E., V. Mantič, and F. París (2007). On the estimation of the first interpenetration point in the open model of interface cracks. *International Journal of Fracture 143*, 287–290.

Hardiman, N. (1954). Elliptic elastic inclusion in an infinite elastic plate. *The Quarterly Journal of Mechanics and Applied Mechanics 7*, 226–230.

Hills, D. and J. Barber (1993). Interface cracks. *International Journal of Mechanical Sciencies 35*, 25–37.

Hull, D. and T. Clyne (1996). *An Introduction to Composite Materials*. Cambridge University Press.

Hutchinson, J. and Z. Suo (1992). Mixed mode cracking in layered materials. *Advances in Applied Mechanics 29*, 63–191.

Kushch, V.I., S. Shmegera, P. Brøndsted, and L. Mishnaevsky (2011). Numerical simulation of progressive debonding in fiber reinforced composite under transverse loading. *International Journal of Engineering Science 49*, 17–29.

Kushch, V.I., S. Shmegera, and L. Mishnaevsky (2010). Elastic interaction of partially debonded circular inclusions. I. Theoretical solution. *International Journal of Solids and Structures 47*, 1961–1971.

Leguillon, D. (2002). Strength or toughness? A criterion for crack onset at a notch. *European Journal of Mechanics, A/Solids 21*, 61–72.

Malyshev, B. and R. Salganik (1965). The strength of adhesive joints using the theory of cracks. *International Journal of Fracture and Mechanics*, 114–128.

Mantič, V. (2009). Interface crack onset at a circular cylindrical inclusion under a remote transverse tension. Application of a coupled stress and energy criterion. *International Journal of Solids and Structures 46*, 1287 – 1304.

Mantič, V., A. Blázquez, E. Correa, and F. París (2006). Analysis of interface cracks with contact in composites by 2D BEM. In M. Guagliano and M. Aliabadi (Eds.), *Fracture and Damage of Composites*, Chapter 8, pp. 189–248. WIT Press, Southampton.

Mantič, V. and F. París (2004). Relation between SIF and ERR based measures of fracture mode mixity in interface cracks. *International Journal of Fracture 130*, 557–569.

Ogihara, S. and J. Koyanagi (2010). Investigation of combined stress state failure criterion for glass fiber/epoxy interface by the cruciform specimen method. *Composites Science and Technology 70*, 143–150.

París, F., E. Correa, and J. Cañas (2003). Micromechanical view of failure of the matrix in fibrous composite materials. *Composites Science and Technology 63*, 1041–1052.

París, F., E. Correa, and V. Mantič (2007). Kinking of transversal interface cracks between fiber and matrix. *Journal of Applied Mechanics 74*, 703–716.

Quesada, D., D. Leguillon, and C. Putot (2009). Multiple failures in or around a stiff inclusion embedded in a soft matrix under a compressive loading. *European Journal of Mechanics, A/Solids 28*, 668–679.

Rice, J. R. (1988). Elastic fracture mechanics concepts for interfacial cracks. *Journal of Applied Mechanics55*, 98–103.

Schmauder, S. and M. Meyer (1992). Correlation between Dundurs' parameters and elastic constants. *Z. Metallkd 83*, 524–527.

Suga, T., G. Elssner, and S. Schmauder (1988). Composite parameters and mechanical compatibility of material joints. *Journal of Composite Materials 22*, 917–934.

Távara, L., V. Mantič, E. Graciani, and F. París (2011). BEM analysis of crack onset and propagation along fiber-matrix interface under transverse tension using a linear elastic-brittle interface model. *Engineering Analysis with Boundary Elements 35*, 207–222.

Taylor, D. (2007). *The theory of critical distances. A new perspective in fracture mechanics*. Oxford: Elsevier B.V.

Toda, H., T. Ueda, K. Toshiro, and A. Takashi (2001). Interfacial debonding criteria under combined stress. *Journal of the Society of Materials Science, Japan 50*, 1375–1381.

Toya, M. (1974). A crack along the interface of a rigid circular inclusion embedded in an elastic solid. *International Journal of Fracture 9*, 463–470.

Xie, M. and A. Levy (2007). Defect propagation at a circular interface. *International Journal of Fracture 144*, 1–20.